Habilitationsschrift

zur

Erlangung der Venia legendi

für das Fach Physik

der

Ruprecht-Karls-Universität

Heidelberg

vorgelegt von

Jörg Evers

aus Castrop-Rauxel

2008

Coherence and interference in quantum optics

Contents

1 Introduction

According to Feynman, quantum interference "has in it the heart of quantum mechanics". Almost all phenomena described by quantum mechanics in one way or another involve interference or the related concept of coherence. This in particular holds true for the field of quantum optics, which is the study and application of the interactions of light with matter at the quantum level. The invention of the laser as a versatile source of coherent light has led to a multitude of fascinating concepts and applications in quantum optics all relying on coherence and interference. Coherence usually can be thought of as a correlation or a fixed phase relation. Examples are the relative phase between two quantum states of an atom (atomic coherence), correlations between different positions in a section through a light beam perpendicular to the propagation axis (transverse coherence) or a fixed phase relation between different positions along the propagation direction of a laser beam (longitudinal coherence). The laser is an indispensable tool in quantum optics not least because it conveniently allows to induce coherences in the studied quantum systems. The relation between coherence and interference effects arises from the fact that quantum interference relies on the presence of different indistinguishable pathways, and depends on the relative phase of the respective pathways. Typically, interference effects vanish if these phases are random, and thus fixed phase relations – coherences – are required for interference to take place.

In this work, different aspects of coherence and interference in quantum optics will be discussed. In analogy to the archetype Young's double slit experiment, Sec. 2 starts by analyzing pathway interference within a single quantum object. In these systems, the respective pathways correspond to different indistinguishable electronic evolutions of the atom. Such analysis is of interest both from a fundamental and from an application point of view. For example, in Sec. 2.1 it turns out that the interference observed is enforced by complementarity of energy and time, rather than position and momentum as in the usual double slit experiments. Thus in this setup, a different class of interference effects can be studied. At the same time, the proposed model system is an ideal candidate to observe so-called spontaneously generated coherences, which despite the huge interest from the theoretical side have not been observed in atomic systems yet. Sec. 2.2 discusses the control of quantum interference via the phases of driving laser fields. For this, the resonance fluorescence spectrum of a three-level system in Λ configuration is studied, where the transition between the two ground states is driven by a strong laser field. In previous work, the driving field was treated classically, which prohibited a clear interpretation of the found results. Here, a quantum treatment enables one to clearly identify the underlying mechanisms such that they could be applied to more complex systems. It turns out that even though the atomic structure is in Λ configuration, interference takes place in V-type subsystems dynamically induced by the quantized driving field.

In the following Sec. 3, light propagation through coherently prepared media is discussed, which is an important application of atom-light interactions, e.g., for the optical processing of information. Based on an atomic coherence effect, electromagnetically induced transparency (EIT), a probe pulse can propagate through a near-resonant medium essentially unattenuated. With EIT, also an extensive control of the group velocity of probe pulses is possible. In Sec. 3.1, light propagation in so-called closed-loop systems is analyzed. This is a particular class of atomic media, where the applied laser fields form a closed interaction loop. These media feature interesting interference effects, but at the same time require a time-dependent analysis as they in general do not evolve into a stationary state. Applications both for the group velocity control and for the non-linear self-phase modulation of light in closed-loop media are discussed. In Sec. 3.2, a system is presented which enables one to control the group velocity of light pulses in the ultra violet frequency domain. This is of importance since ongoing advancement of laser technology extends the operational range of lasers to higher and higher frequencies. Thus, the need for optical elements that operate beyond the visible frequency range arises. Dispersive quantum optical media could

be an interesting alternative to conventional optical elements. The last subsection 3.3 demonstrates that closed-loop atoms are an ideal candidate to realize media with a negative index of refraction in atomic gases. In particular, metastable neon is identified as a promising model system to achieve lossless negative refraction or even active, amplifying negative index media. Different aspects of the calculation, such as the treatment of dense atomic gases and the chiral response of the medium to the applied probe field, are discussed.

A difference to classical double slit experiments and realizations in atomic systems arises due to the internal structure of the atoms. This leads to vanishing interference fringe visibility in light scattering of strong driving fields off of regular structures of atoms, which hampers applications. In Sec. 4, it is demonstrated how the interference can be recovered at strong driving, and the properties of the scattered light are analyzed in detail. The key idea here is to modify the mode density of the electromagnetic vacuum field, causing a redistribution of the relevant dressed state populations in the driven atoms. This can be done in such a way that the coherent nature of the scattered light is recovered, and that quantum interference in the scattered light can take place.

In the next Sec. 5, coherence and interference effects in interacting ensembles of atoms are discussed. The first part Sec. 5.1 focusses on an exact treatment of the dipole-dipole interaction of a pair of atoms, with the emphasis on the geometrical structure of this coupling, and on interactions between transitions with orthogonal dipole moments. It is shown that the geometry alone can crucially influence the electronic dynamics of the system. Depending on the relative orientation of two atoms, the system either evolves into a time-independent stationary state or not. Further analysis based on these results leads to the conclusion that the few-level approximation in general is invalid in collective systems. Rather, the involved atoms must be modelled using complete Zeeman manifolds in order to guarantee correct results. As an application for the extended level space, decoherence-free subspaces in collective multilevel systems are discussed. The second part Sec. 5.2 analyzes coherent control of many-particle systems in the Dicke limit. As the main applications, it is demonstrated how an ensemble of atoms driven only by an incoherent thermal bath can be used as a versatile source of nonclassical light.

Complementary to the tremendous process in advancing quantum optics to a precision science in the frequency and time domain for example with applications for optical clocks, in Sec. 6 precision schemes in the spatial domain are discussed. The first part deals with the sub-wavelength position determination for a single atom. Multiple simultaneous measurements are facilitated in order to improve the spatial resolution, or to achieve multidimensional localization. In the second part, the localization of a small ensemble of interacting particles based on the collective quantum dynamics of the sample is discussed. In Sec. 6.1.3, a scheme to measure interatomic distances far below the classical resolution limit is presented. Finally, in Sec. 6.2, it is shown how resonant interferometric lithography can be used to write structures with feature size smaller than the employed light wavelength.

It is interesting to note that in most cases, quantum optical models are abstractions that do not exclusively refer to atomic systems. Therefore, in the last Sec 7, the extension of quantum optical schemes to nuclear physics is discussed. Upcoming high-frequency free-electron lasing facilities allow to near-resonantly drive selected nuclei, such that one may hope to extend the extensive control schemes of atomic quantum optics to nuclear physics. These laser sources, however, suffer from a limited coherence length of the light pulses, such that the partial coherence must be considered in the theoretical modelling. Both near-resonant and off-resonant driving with super-intense laser fields are discussed, together with applications in triggering the controlled de-excitation of nuclear isomers.

2 Pathway interference within atoms

2.1 Interference in the time-energy domain

Quantum interference is a powerful tool to change the dynamics of an atomic system. This especially holds true if the interference takes place within the studied quantum object itself. A particular class of such internal interferences are related to the so-called spontaneously generated coherences (SGC). These arise if an atom emits a (virtual) photon on one transition in such a way that the photon does not leave the atom, but rather is absorbed on a different transition in the same atom, see Fig. 1(a). This process is related to the self-energy leading, e.g., to the Lamb shift, where photon emission and absorption take place on the same transition [Fig. 1(b)], and to the dipole-dipole interaction where the photon is emitted and absorbed by different particles, see Fig. 1(c). Spontaneously generated coherences have been studied in numerous theoretical works due to their fascinating applications [Fic05], but so far in atomic systems, there is only a single experiment [Xia96], which furthermore could not be verified in a repetition of the experiment [Li00]. SGC have been observed, however, in artificial quantum systems [Dut05]. The reason for this lack of experimental confirmation is the stringent conditions on the atomic structure for SGC to take place. The two involved transitions must be near-degenerate and must have non-orthogonal transition dipole moments. Loosely speaking, the emitted virtual photon has to match the absorbing transitions. In real atoms, this cannot be fulfilled, for example, the commonly studied V- or Λ-type level schemes of Fig. 1(a).

The conditions are fulfilled, however, in a four-level system in $J = 1/2 \leftrightarrow J = 1/2$ configuration as shown in Fig. 2(a), by the two π-transitions preserving the magnetic quantum number m_j. This level structure can be found, e.g., in mercury ions [26, 29]. Light scattering from trapped mercury ions has already been studied experimentally [Eic93a, Ita98]. But in the $J = 1/2 \leftrightarrow J = 1/2$ system, the two π transitions do not share common states, and thus it is not clear if an atom can absorb photons on the one transition after having emitted on the other transition. On the other hand, one finds that in the equations of motion, there are indeed terms which resemble typical SGC contributions. Thus the question arises whether SGC and vacuum-induced interferences take place in this realistic system.

This question can be addressed by assuming that the two π-transitions are driven by a single laser field and by calculating the fluorescence intensity and the fluorescence spectrum emitted on these transitions. Both can be calculated in terms of the steady-state two-time correlation function

$$\left\langle [\vec{e}_z \cdot \hat{E}^{(-)}(\vec{r}, t+\tau)][\vec{e}_z \cdot \hat{E}^{(+)}(\vec{r}, t)] \right\rangle_{t\to\infty} ,$$

where $\hat{E}^{(\pm)}$ are the positive and negative frequency part of the quantized electromagnetic field, $\vec{r}$ is the detector position, and $\vec{e}_z$ is the unit polarization vector. The fluorescence intensity follows with $\tau = 0$, and it is found that it is not affected by SGC

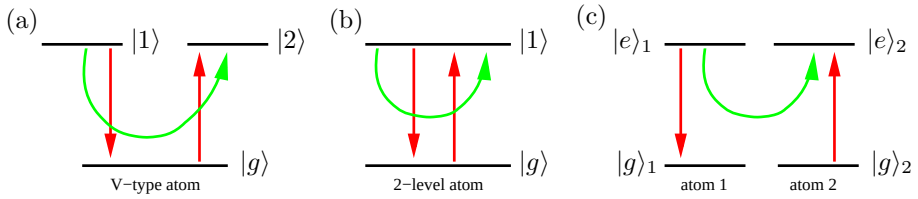

Figure 1: Vacuum-induced processes contributing to (a) spontaneously generated coherences, (b) the self energy, and (c) the dipole-dipole interaction between two atoms. The green arrow denotes the vacuum-mediated population transfer, the red arrows indicate the involved atomic transitions.

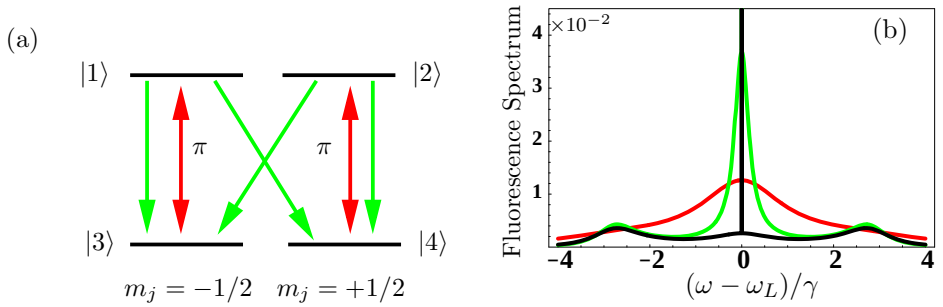

Figure 2: (a) 4-level atom in $J = 1/2 \leftrightarrow J = 1/2$ configuration as found, e.g., in mercury ions. The green lines denote spontaneous emission channels, the red line indicates coherent driving with frequency ω_L on the so-called π transitions. (b) Resonance fluorescence spectrum emitted from the π transitions. The black line shows the complete fluorescence spectrum for perfect detector resolution. The green line is the spectrum with interference terms artificially omitted. The vertical line at $\omega = \omega_L$ denotes the elastic Rayleigh peak that is present both with and without interference terms. If observed with a finite frequency resolution of order of the natural decay rate γ, the spectra with and without interference terms are virtually identical (red line).

or interference, because the terms in the equations of motion turn out to be proportional to $\langle |1\rangle\langle 3|\,|4\rangle\langle 2|\,\rangle_{t\to\infty}$ which is zero because of the orthogonality of the ground states. Thus, the more general level scheme suppresses the SGC contributions in the equations of motion as suspected above.

But in contrast, surprisingly the fluorescence spectrum does show signatures of interference, as can be seen from Fig. 2(b). A closer analysis reveals that for the spectrum, the two operators $|1\rangle\langle 3|$ and $|4\rangle\langle 2|$ have to be evaluated at different times, $\tau \neq 0$. Then, they are no longer orthogonal and the SGC contributions can contribute. Thus, it can be concluded that the presented system indeed is a realistic setup to verify the as yet unobserved presence of SGC in atomic systems [26].

But perhaps even more interesting, the interpretation of the results reveals that they arise from complementarity of energy and time [29]. If the observer decides to measure the total intensity, then the detector does not detect the energies of the different photons. Since there is no spectral information, complementarity does not impose any restrictions on the time resolution of such a measurement, and hence it is in principle possible to detect the photons in a time resolved way. Thus the experimental conditions allow, at least in principle, to determine the atomic ground state immediately after the detection of a π-photon. This implies that the π-photons cannot interfere, since one could decide on which of the two π-transitions the photon was emitted and hence reveal the quantum path taken by the system.

This completely changes if the spectrum of resonance fluorescence is measured. Here, the observer decides to measure the photon energies precisely. Since time and energy are complementary observables, no information on the time sequence of the emission can be obtained simultaneously, and the photon emission times are indeterminate. In contrast to the measurement of the total intensity, it is now impossible to decide on which transition the π-photon has been emitted, such that different indistinguishable pathways are possible. Therefore, the SGC can contribute and interference occurs. A similar argument explains why interference was observed in a recent attosecond time-energy double-slit experiment [Lin05a], where the spectral resolution of the detector makes the "time slits" indistinguishable.

An quantitative analysis is possible in terms of the time-energy uncertainty relation, supported by a calculation for spectral measurements with variable frequency resolution. Also, a dressed-state analysis allows to clearly identify the interfering pathways, further supporting the above interpretation [26, 29].

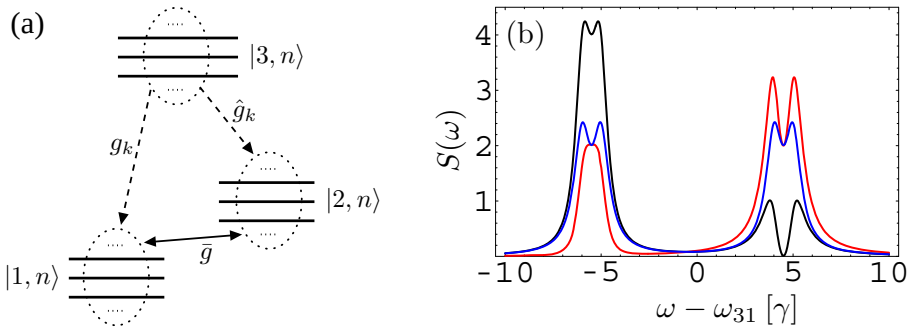

Figure 3: (a) The considered Λ-type system. The multiple lines for each state denote the Fock state multiplets induced by the coupling of the atom with a quantized driving field. The upper states $|3,n\rangle$ decay spontaneously into the two lower state multiplets $|1,n\rangle$ and $|2,n\rangle$. Here, n is the number of photons in the respective driving field Fock modes. The two lower state multiplets are coupled by the quantized driving field. g_k and $\hat{g}_k$ are coupling constants for the interaction with the vacuum giving rise to spontaneous emission, $\bar{g}$ is the coupling constant for the driving field. (b) Spontaneous emission spectrum. The black and the red line indicate spectra for different driving field phases in the phase-dependent system. The blue curve is the result for the phase-independent system, and can also be obtained by averaging over all phases.

2.2 Phase control of quantum interference

Quantum interference relies on the interplay of different pathways from one initial to a final state. The outcome of the interference of the different pathways crucially depends on the relative phases of the different pathways, as already found in Young's double slit experiment. This in principle also holds true for laser-field induced pathways, even though it is experimentally challenging to control the phase of laser fields in atom-field interactions. In particular at optical frequencies, usually only the relative phase between two laser fields can be controlled, for example, because the phases depend on the distance between the laser source and the driven atom. Nevertheless, the influence of the relative phase on the quantum dynamics of an atomic system has been studied experimentally [Kor99b].

Among the simplest examples for a phase-sensitive system is a three-level system in Λ configuration, as shown in Fig. 3(a) [Mar97]. The transition dipole moments from the upper state to the two lower states are assumed to be non-orthogonal, giving rise to interference effects as discussed in the last Sec. 2.1. It is easy to show that this system depends on the phase of the control field coupling the two ground states, such that, for example, the spontaneous emission spectrum becomes asymmetric and phase-dependent. In Fig. 3(b), the emission spectrum is shown for two different driving field phases (black and red curves). The blue curve is the reference obtained if the phase-dependence is ignored.

This phase dependence is usually attributed to the fact that due to the driving field, each of the two lower states can be reached via two pathways: Either by a direct spontaneous decay, or by a decay into the other state followed by a driving field-induced transition. The two paths interfere, with a relative phase between the two path amplitudes equal to the driving field phase. This classical interpretation, however, is unsatisfactory. First of all, the respective initial and the final states of two interfering pathways are obviously not the same, as one involves an interaction with the driving field, whereas the other does not. Thus one could argue that the two paths do not interfere, as they could be distinguished by a measurement. A typical counter-argument against this is that the photon number distribution of a strong coherent driving field has a large width, such that the two paths cannot be distinguished. This argument, however, cannot be verified using a semi-classical description of the system.

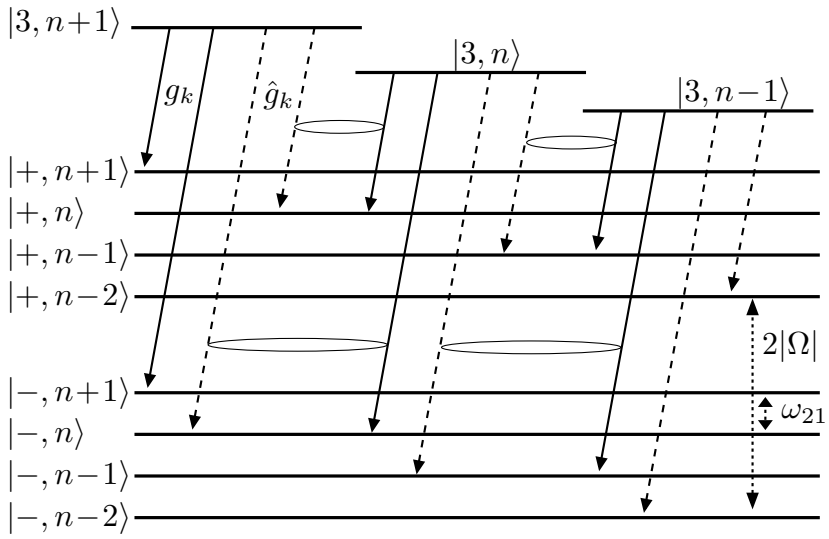

Figure 4: Decay pathways starting from single upper state Fock modes $|3,n\rangle$ into the corresponding lower dressed states. The solid (dashed) arrows are decays due to coupling via coupling constant g_k ($\hat{g}_k$). The ellipses mark interfering pathways. The parameters are chosen such that the AC-Stark splitting $|\Omega|$ is larger than the photon frequency splitting ω_{21}, as indicated by the double arrows.

Also, while it is clear that the two pathways must have either a different initial or a different final state, it is not apparent in the semiclassical description what the exact pathways are.

These problems can be resolved with a fully quantized treatment of the problem, as it is indicated by the different photon number states $|n\rangle$ of the quantized control field coupling states $|1\rangle$ and $|2\rangle$ in Fig. 3(a) [22]. The spontaneous emission spectrum can be explained with the help of the dressed states with respect to the field coupling $|1\rangle$ and $|2\rangle$,

$$|+,n\rangle = \frac{1}{\sqrt{2}}\left(|1,n+1\rangle + i\,e^{i\phi}\,|2,n\rangle\right)\,, \tag{1a}$$

$$|-,n\rangle = \frac{1}{\sqrt{2}}\left(|1,n+1\rangle - i\,e^{i\phi}\,|2,n\rangle\right)\,, \tag{1b}$$

where ϕ is the phase of the control field. The four transitions between the dressed states correspond to the four peaks seen in the blue reference curve without interference in Fig. 3(b).

The quantized treatment of the driving field allows to explore the effect of non-classical driving fields, and thereby determine the origin of the quantum interference. It is found that for a driving field which consists of a single Fock number state mode, no interference effects are present. Similarly, a driving field which is a superposition of many non-adjacent Fock modes dos not induce any interference effects. Here, non-adjacent means that the modes are such that if Fock state $|n\rangle$ is populated, then the adjacent modes $|n\pm1\rangle$ are not populated. Finally, if two adjacent Fock modes are populated, then interference and thus phase-dependence appears, and if the range of populated adjacent Fock states increases, the classical result with full phase-dependence is approached.

This behavior can be understood from Fig. 4, which shows a dressed-state representation of the system. It is important to note that even though the driving field is assumed to couple the two lower states only, in the energy spectrum, the upper state atomic state $|3\rangle$ also splits up in a multiplet of states $|3,n\rangle$ which decays into the corresponding dressed states. Fig. 4 shows all the possible decay pathways from

three adjacent upper states $|3, n+1\rangle$, $|3, n\rangle$ and $|3, n-1\rangle$. First, only state $|3, n\rangle$ is assumed to be populated, i.e. a single Fock mode. Then Fig. 4 shows that each of the possible final states is only reached via a single pathway from the initial state. Thus no interference is possible. Next all three adjacent upper states $|3, n\rangle$ and $|3, n \pm 1\rangle$ are assumed populated. Then some of the final states can be reached via two pathways, as indicated by the ellipses in Fig. 4, which gives rise to the studied interference and phase effects. It is interesting to note that the two initial states of the interfering pathways are different, only the final state is the same. The two initial states, however, have a fixed phase relation with relative phase ϕ, which nevertheless allows for interference to take place. The interfering subsystems are thus independent three-level systems in V configuration, even though the initial level structure is a Λ-type system. This conclusion can be further verified by noting from Fig. 4 that for each final state, one of the pathways is mediated by the coupling constant g_k, whereas the other path is proportional to $\hat{g}_k$. Thus the interference effects should also be controllable via the relative phase of these coupling constants just as via the phase ϕ. A numerical check shows that this is indeed the case.

A closer analysis shows that the laser-induced V-type subsystems are not entirely equivalent to a three-level $V-$-type atom with parallel dipole moments, in that different conditions for maximum interference must be fulfilled. The analysis further enables one to identify the correct treatment of the quantized driving field phase [22].

3 Light propagation in coherently prepared media

One of the most important applications of light-matter interaction both from a fundamental and from an application point of view is the propagation of a light pulse through a dispersive medium. A landmark achievement in this area that fueled much of the following work was the realization that laser-induced atomic coherence in the form of electromagnetically induced transparency (EIT) could be used to propagate a probe pulse through a near-resonant medium essentially unperturbed [Har97]. In particular, the modification of the group velocity of a probe field pulse has received considerable attention. Based on EIT, also the group velocity of probe pulses can be controlled to a great extend, including a complete stopping of light in a suitably prepared medium [Fle05].

The group velocity v_g of probe pulses in dispersive media is essentially determined by the slope of the real part of the susceptibility [Fic05],

$$v_g = \frac{c}{n'(\omega_p) + \omega_p/[2n'(\omega_p)]\,\frac{\partial \chi'(\omega_p)}{\partial \omega_p}}\,. \tag{2}$$

Here, n' and χ' are the real parts of the index of refraction and the susceptibility, and ω_p is the probe field frequency. Typically, the derivative part dominates the denominator for applications in group velocity control. If the derivative part is large and positive, then $v_g \ll c$, and slow (subluminal) light propagation is achieved. If the derivative part is negative, then either $v_g > c$ (superluminal propagation) or $v_g < 0$ (negative group velocity) are possible. It should be noted that only in some cases, the group velocity coincides with the velocity at which information can be sent, such that causality is always preserved. All cases have been realized in coherently prepared atomic media, and the susceptibility and thus the group velocity can be calculated from the atomic probe field transition coherence.

3.1 Beyond the multiphoton resonance condition

A particular class of atomic media are so-called loop media [Koc90, Kei93, Mor02, Kor99a], in which a certain initial atomic state is connected to another atomic state via several different combinations of laser field interactions. For example, starting from state $|1\rangle$ in Figure 5, it is possible to evolve the atomic population by laser fields via

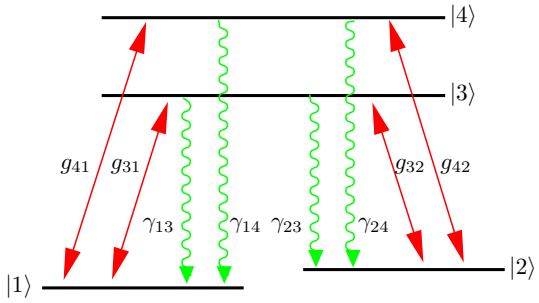

Figure 5: The four-level double-Λ type schemes considered in the analysis, driven by four laser fields indicated by the red arrows with Rabi frequencies g_{ij} ($i \in \{3,4\}$, $j \in \{1,2\}$). The laser configuration forms a closed interaction loop. This loop gives rise to a dependence on the relative phase of the different laser fields, and in general makes a time-independent steady state of the system dynamics impossible. The spontaneous decays with rates γ_{ij} are denoted by the wiggly green lines.

states $|3\rangle$, $|2\rangle$ and $|4\rangle$ back to the initial state $|1\rangle$, such that the condition for a closed-loop system is fulfilled. This greatly affects the optical properties since the different possible pathways can interfere [22]. On the other hand, closed-loop systems in general do not have a time-independent stationary state. A steady state is reached only if a particular linear combination of the detunings of all incident laser fields is zero, that is, if the so-called multiphoton resonance condition is fulfilled. This assumption was made in previous studies, but is invalid for pulse propagation analysis, because a probe pulse which is finite in time necessarily consists of different frequency components which cannot fulfill the multiphoton condition simultaneously. Therefore, a time-dependent study beyond the multiphoton resonance condition is required [24, 50].

In the considered model system depicted in Figure 5, the probe field is applied to transition $|1\rangle \leftrightarrow |4\rangle$. Mathematically, the closed-loop property implies that it is impossible to find an interaction picture in which the Hamiltonian does not have an explicit time dependence. The simplest form for the Hamiltonian V is

$$\begin{aligned} V =& \hbar(\Delta_{32} - \Delta_{31})\tilde{\rho}_{22} - \hbar\Delta_{31}\tilde{\rho}_{33} + \hbar(\Delta_{32} - \Delta_{31} - \Delta_{42})\tilde{\rho}_{44} \\ & - \hbar\left(g_{31}\tilde{\rho}_{31} + g_{32}\tilde{\rho}_{32} + g_{42}\tilde{\rho}_{42} + g_{41}\tilde{\rho}_{41}e^{-i\Phi} + \text{ h.c.}\right). \end{aligned} \tag{3}$$

Here, $\tilde{\rho}_{ij}$ is the operator $|i\rangle\langle j|$ in the chosen reference frame ($i, j \in \{1, \ldots, 4\}$). The Rabi frequencies are g_{ij}, and Δ_{ij} are laser field detunings. In this interaction picture, the residual time dependence along with the laser field phases appears only together with the probe field Rabi frequency g_{41} in the parameter Φ given by

$$\Phi = \Delta t - \vec{K}\vec{r} + \phi_0\,, \qquad \Delta = (\Delta_{32} + \Delta_{41}) - (\Delta_{31} + \Delta_{42})\,, \tag{4a}$$

$$\vec{K} = (\vec{k}_{32} + \vec{k}_{41}) - (\vec{k}_{31} + \vec{k}_{42})\,, \qquad \phi_0 = (\phi_{32} + \phi_{41}) - (\phi_{31} + \phi_{42})\,. \tag{4b}$$

The parameters Δ, $\vec{K}$ and ϕ_0 are known as the multiphoton resonance detuning, wave vector mismatch and initial phase difference, respectively. These parameters are a direct consequence of the closed-loop nature. In general it is not possible to find a reference frame where the explicit time dependence due to Δ vanishes from the Hamiltonian, such that for $\Delta \neq 0$ no stationary long-time limit can be expected. Therefore, a time-dependent solution of the density matrix equations is required. Using the notation $\bar{g}_{41} = g_{41}\exp[-i\vec{K}\vec{r} + i\phi_0]$, the density matrix equations of motion can be written as

$$\frac{\partial}{\partial t}\tilde{R} + \Sigma = M\tilde{R}, \tag{5}$$

where $\tilde{R}$ is a vector containing the density matrix elements. M is a time-dependent matrix, and Σ a time-dependent vector independent of the density matrix elements which

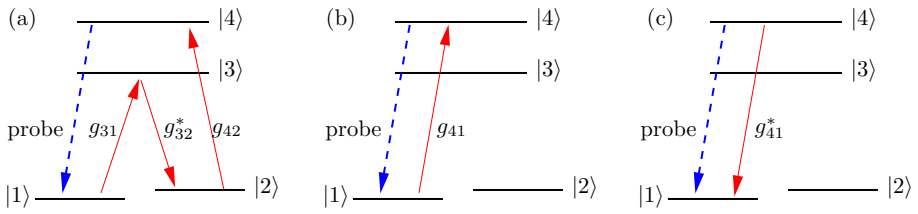

Figure 6: Interpretation of the different contributions to the probe field susceptibility in terms of transition pathways. (a) represents the interaction loop leading to a scattering of the driving fields into the probe field mode. (b) is the direct scattering of the probe field off of the probe transition. (c) shows a counter-rotating term. The solid red arrows indicate coupling field transitions, the dashed blue line is a probe field interaction.

arises from eliminating one of the state populations from the equations of motion via the trace condition $Tr(\tilde{\rho}) = 1$. For a weak probe field, using Floquet's theorem [Flo83], the solution $\tilde{R}$ can be obtained with a series ansatz

$$\tilde{R} = \tilde{R}_0 + \bar{g}_{41} e^{-i\Delta t} \tilde{R}_1 + \bar{g}_{41}^* e^{i\Delta t} \tilde{R}_{-1} + \dots , \tag{6}$$

where $\tilde{R}_i$ ($i \in \{0, \pm 1, \dots\}$ are time-independent coefficient vectors. Using this ansatz, the time-dependent solution to the density matrix equations of motion can be found, which allows to evaluate all observables [24, 50].

3.1.1 Linear response: Group velocity control

In an interaction picture oscillating in phase with the applied probe field, the probe field transition coherence $\hat{\rho}_{41}$ determining the light pulse propagation through the medium can be written as,

$$\hat{\rho}_{41} = [\tilde{R}_0]_{13}\, e^{i\Phi} + g_{41}[\tilde{R}_1]_{13} + g_{41}^*[\tilde{R}_{-1}]_{13}\, e^{2i\Phi} , \tag{7}$$

where $[x]_{13}$ denotes the relevant 13th component of the vector x [24]. The different contributions to this result naturally arising from the Floquet analysis correspond to the various involved physical processes and allow to in detail understand the medium response.

The first part of Eq. (7) represents the scattering of the driving fields into the probe field mode arises from $[\tilde{R}_0]_{13}$, as shown in Fig. 6(a). This contribution in general does not oscillate at the probe field frequency, but rather at the combination frequency $\omega_{31} + \omega_{42} - \omega_{32}$ of the three driving fields. This frequency coincides with the probe field frequency only under multiphoton resonance. The contribution proportional to $[\tilde{R}_1]_{13}$ shown in Fig. 6(b) is in phase with the probe field for all values of Δ, and is independent of the relative field phase. It represents the direct scattering of the probe field off of the probe field transition. The third contribution proportional to $[\tilde{R}_{-1}]_{13}$ can be interpreted as a counter-rotating term which in the Floquet expansion differs by 2Δ from the probe field frequency, and is depicted in Fig. 6(c).

As an important result, it can be concluded that the phase-dependence of the loop-configuration studied here is restricted to the multiphoton resonance condition $\Delta = 0$, because it arises from the scattering of the coupling fields into the probe field mode. Furthermore, it can be seen from Eq. (7) that all contributions but the direct scattering acquire an additional dependence on the wave vector mismatch $\vec{K}$ together with the dependence on the phase ϕ_0. Therefore, the laser field geometry influences the relevance of these contributions to the detection signal in probe field propagation direction. In general, only the direct scattering contribution can be detected in propagation direction of the probe beam regardless of the separation of detector and the scattering atoms.

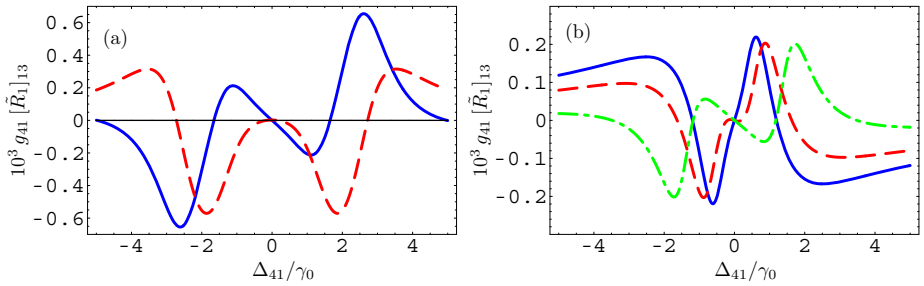

Figure 7: (a) Real (blue solid line) and imaginary (red dashed line) parts of the contribution to the Floquet decomposition representing the direct scattering of the probe field off of the probe transition, $g_{41}\,[\tilde{R}_1]_{13}$ against the probe field detuning Δ_{41}. This corresponds to a calculation relevant for the evaluation of the group velocity, but violates the multiphoton resonance condition and thus requires a Floquet analysis. The parameters are $\Delta_{31} = \Delta_{32} = \Delta_{42} = 0$, $2\gamma_{13} = 2\gamma_{14} = 2\gamma_{23} = 2\gamma_{24} = \gamma_0$, $g_{31} = 2\gamma_0$, $g_{32} = 0.1\gamma_0$, $g_{42} = 0.8\gamma_0$, and $g_{41} = 0.01\gamma_0$. (b) Real part of the Floquet contribution $[\tilde{R}_1]_{13}$ [see Eq. (7)] as in (a). The solid blue line is for $g_{31} = 0.7\gamma_0$, the red dashed line for $g_{31} = 0.85\gamma_0$, and the green dash-dotted line for $g_{31} = 1.5\gamma_0$. The other parameters are $\Delta_{31} = \Delta_{42} = 0$, $g_{32} = 0$, $2\gamma_{13} = 2\gamma_{14} = 2\gamma_{23} = 2\gamma_{24} = \gamma_0$, $g_{42} = 0.2\gamma_0$, and $g_{41} = 0.01\gamma_0$.

The considered system enables one to control the pulse propagation to a great extend. In Fig. 7(a), the probe field susceptibility is shown against the probe field detuning Δ_{41}, while the coupling field detunings are $\Delta_{31} = \Delta_{32} = \Delta_{42} = 0$. This corresponds to a calculation relevant for the evaluation of the group velocity, but violates the multiphoton resonance condition $\Delta = 0$ for most values of Δ_{41} shown in the figure and thus requires the use of the time-dependent Floquet analysis. Consequently, only the component oscillating in phase with the probe field is shown. It can be seen in Fig. 7(a) that around $\Delta_{41} = \pm 2\,\gamma_0$, the real part of the susceptibility has positive slope, while the imaginary part is strongly negative. This indicates subluminal light propagation with gain. At about $\Delta_{41} = 0$, the real part of the susceptibility has negative slope over a wide frequency range, together with a small positive or even negative imaginary part. This corresponds to superluminal propagation with small absorption or gain.

For suitable parameters, the light propagation can conveniently be controlled via one of the coupling field Rabi frequencies, as shown in Fig. 7(b). The different curves correspond to different Rabi frequencies on transition $|3\rangle \leftrightarrow |1\rangle$. At resonant probe field $\Delta_{41} = 0$, for the parameters in this figure the absorption vanishes for all three curves [24].

3.1.2 Non-linear response: Self-phase modulation

The double-Λ system also offers interesting prospects for non-linear light-matter interactions, with applications as beam focussing, pulse compression, phase modulation or optical switching [Boy92]. For example, in addition to the linear index of refraction, stronger probe fields experience a nonlinear index of refraction, which induces a so-called self-phase modulation given by

$$\Delta\Phi_{\mathrm{NL}} = n_2 I k L\,,$$

where n_2 is the non-linear index of refraction, I the probe field intensity, k the probe field wave vector and L the propagation length. In the following, the self-phase modulation is evaluated for the given double-Λ system using realistic parameters for hot a sodium vapor [50]. The analysis includes Doppler and pressure broadening, as well as argon as a buffer gas to compensate for the large Doppler broadening. As in Sec. 3.1.1,

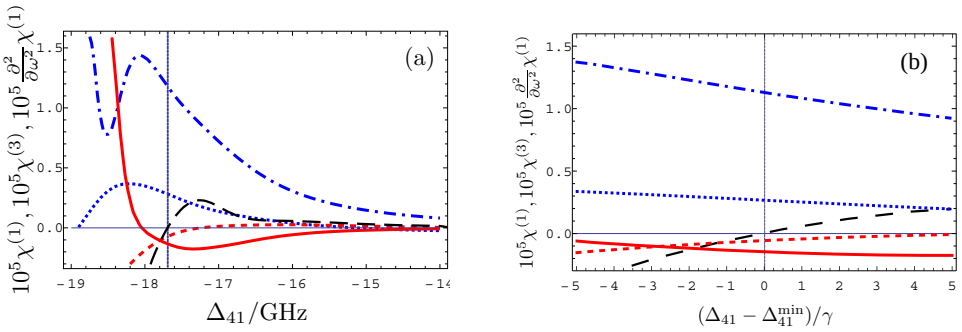

Figure 8: (a) Real part (dash-dotted blue line) and imaginary part (solid red line) of the nonlinear susceptibility together with the real part (blue dotted line) and the imaginary part of the linear susceptibility (dashed red line). The sodium gas has a temperature of $T = 548$ K, which leads to a density $N = 1.0 \times 10^{20}$ m^{-3} and a Doppler linewidth of $\delta\omega = 2\pi \times 1.78$ GHz. The argon buffer gas has a density of $N_b = 3.95 \times 10^{23}$ m^{-3}. The control fields have Rabi frequencies $g_{42} = 60$ GHz, $g_{31} = 30$ GHz, $g_{32} = 25$ GHz, and the detunings are $\Delta_{31} = 1.6$ GHz, $\Delta_{32} = \Delta_{42} = 0$. The solid black line shows the second derivative of the real part of the linear susceptibility required to calculate the group velocity dispersion. (b) Magnification of the relevant part of (a).

a time-dependent Floquet analysis is required, but including higher-order contributions to evaluate the nonlinear response. Doppler broadening in a hot vapor effectively leads to an additional velocity-dependent detuning which can be modelled by averaging the results over a Gaussian velocity distribution. The buffer gas causes frequent collisions between the different vapor particles and effectively leads to an additional decay of the atomic coherences. Co-propagating driving and probe laser fields were found to be most advantageous as in standard electromagnetically induced transparency.

The real and imaginary parts of the linear and non-linear index of refraction are shown in Fig. 8(a). At the probe field frequency $\Delta_{41}^{\min}$ indicated by the vertical solid black line, the imaginary parts of the linear and non-linear indices of refraction are about an order of magnitude smaller than the real part of the non-linear index of refraction. Also, their sign indicates small gain rather than losses. At a slightly higher frequency, the linear and non-linear imaginary parts have opposite signs, such that a cancelling of the respective linear absorption and non-linear gain could be possible.

In both cases, significant non-linear effects can be observed in pulse propagation without significant distortion of the probe pulse. Assuming a probe field strength of 10% of the smallest control field strengths, a non-linear self-phase modulation of π is found to occur after a propagation of about 6.4 cm through the sodium gas.

Fig. 8(b) shows a magnification of the relevant part around $\Delta_{41}^{\min}$. A closer analysis shows that the non-linear self-phase modulation could be observed for pulses with a spectral width of several natural linewidths of the considered sodium D_1 transition $\gamma = 2\pi \times 9.76$ MHz. In the same region, group velocity dispersion is low such that pulse shape distortions can be expected to be small.

3.2 Group velocity control in the ultraviolet domain

Recent advancement in technology allows to extend the frequency range at which lasers are available to higher and higher frequencies. This raises the need for optical elements at frequencies beyond visible light, a question that in particular at very high frequencies has not been answered so far. An interesting alternative to conventional optical elements could be dispersive quantum optical systems, if the control schemes known for the optical frequency range can be extended to higher frequencies. In this section, it will be shown that group-velocity control as required, for example, for optical delay lines, can be extended to the ultraviolet frequency region [46].

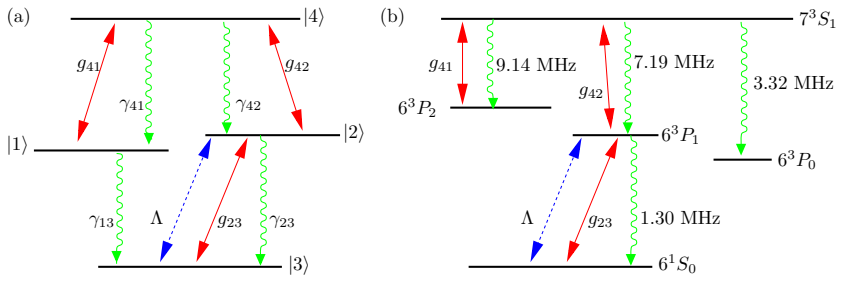

Figure 9: Level scheme for group velocity control in the ultraviolet frequency region. (a) Schematic setup. Red arrows indicate coherent fields, and the probe transition is $|3\rangle \leftrightarrow |2\rangle$. Green arrows denote spontaneous emission, and the blue arrow is an incoherent bidirectional pumping rate. (b) Possible realization in mercury.

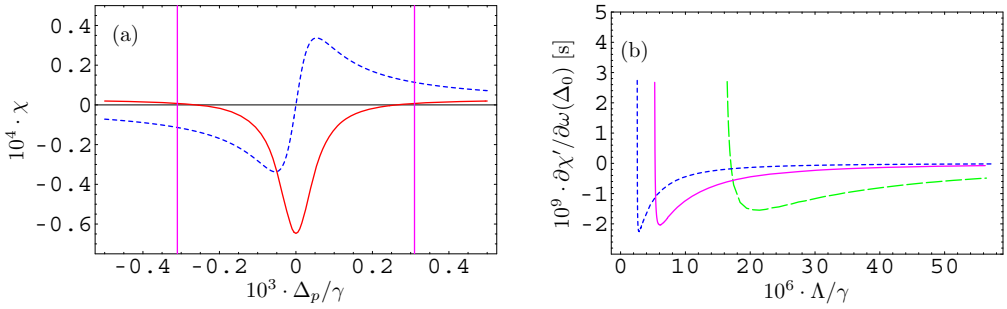

Figure 10: (a) Real (dashed blue) and imaginary (solid red) parts of the probe field susceptibility for probe field detunings Δ_p close to the interacting dark state resonance. The negative sign of the imaginary part indicates gain. (b) Slope of the real part of the susceptibility for different incoherent pump rates Λ. The three curves correspond to different coupling field strengths on transition $|4\rangle \leftrightarrow |2\rangle$. This slope determines the group velocity of pulses propagating through the medium, and can be controlled over a wide range via Λ.

The required atomic level scheme can be found, e.g., in mercury [Fry00]. Both a schematical and a realistic implementation are shown in Fig. 9. The probe field is applied to transition $|2\rangle \leftrightarrow |3\rangle$. The atomic structure is essentially a three-level electromagnetically induced transparency (EIT) system in ladder configuration consisting of states $|2\rangle$, $|3\rangle$ and $|4\rangle$. This subsystem alone exhibits EIT, albeit imperfect due to the negative effect of the spontaneous emission. In addition, a perturbing state $|1\rangle$ is weakly coupled to the system. This gives rise to a very narrow peak structure in the optical response curves, due to an interference effect which has been termed interacting dark state resonance in the literature [Luk99].

As explained in Sec. 3.1.1, resonance structures like the interacting dark state resonance are of great interest for the control of the group velocity v_g of probe pulses, as they imply a strong frequency dependence of the optical response. It turns out that the properties of the interacting dark state resonance can be controlled via an additional incoherent pump rate on the probe field transition [Fry00] [46]. Usually, the dark state resonance is absorptive, but increasing the incoherent pumping, a population inversion on the relevant dressed states is achieved such that the probe transition becomes amplifying. As an example, the real and the imaginary part of the probe field susceptibility around the narrow structure induced by the perturbing field are shown in Fig. 10(a). Note that unlike typical EIT structures, the width of the structure is only about $10^{-3}\gamma$, where γ is a natural decay rate in the system.

In Fig. 10(a), two frequency ranges which are of interest for pulse propagation are indicated by the vertical purple lines. Around these frequencies, the medium absorp-

tion is low or even vanishes. In Fig. 10(b), the slope of the real part of the susceptibility is shown for different incoherent pump field strengths at this frequency of vanishing absorption. It can be seen that by varying the incoherent pump field strength, the system can be transferred from superluminal light propagation to subluminal light propagation without absorption. In this figure, the respective curves correspond to different coupling field strengths. The strong dependence already on a very weak incoherent pumping suggests sensitive control, e.g., in light switching schemes.

While the interacting dark state resonances offer interesting perspectives for the group velocity control in the ultraviolet domain, one has to keep in mind that the supported frequency width is narrow. Thus, the pulses must not be too short, such that their frequency spectrum is supported by the resonance. One might be tempted to conclude that Doppler broadening would completely wash out the resonance in an experiment. But despite the low width of the structure, an implementation in Doppler-broadened gases is possible. Using co-propagating laser fields, all relevant results of this section can be recovered, and the narrow interacting dark state resonance persists [46].

3.3 Lossless negative refraction in dense atomic gases

Media with a negative index of refraction promise a multitude of fascinating applications such as perfect lenses or improvement in antenna design [Sha07]. But also from a conceptual point of view, negative refraction is of great interest. First of all, the results obtained with negative refractive media often challenge the physical intuition gained in daily life, for example, in computer simulations of images of object falling into a liquid with negative refractive index [Weg]. But more general, negative refractive media pave the way towards quantum optics with magnetic fields.

Negative refraction is typically requires coupling of both the magnetic and the electric field component of a single electromagnetic probe field to the medium. The challenge is thus to provide a medium with sufficient electric and magnetic response at the same frequency. So far, experiments focus on metamaterials, which are artificial structures that can be designed in such a way that the desired electromagnetic response is achieved. Tremendous progress has been achieved, mostly related to the ongoing miniaturization of such artificial structures. Current designs for high-frequency metamaterials, however, are essentially two-dimensional, lossy, and hard to fabricate, which hampers potential applications.

As an alternative approach, negative refraction has recently been predicted in a dense gas of atoms (see, e.g., [K̈07]). Gases are naturally extended, and the probe frequency is limited by the availability of suitable atomic systems rather than by the feature size of nano-fabrication methods. The proposed systems, however, up to now have in common with the metamaterials that they are passive and lossy.

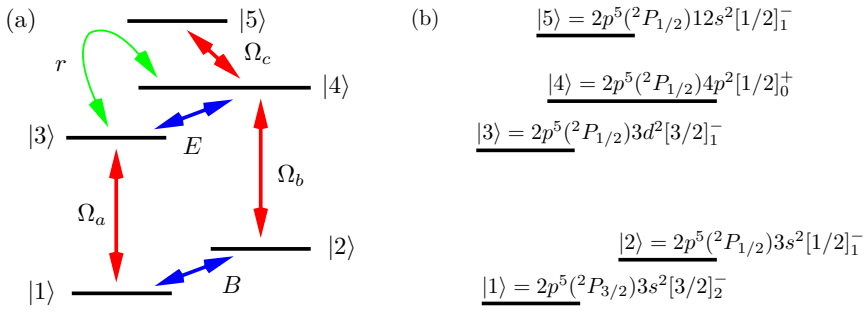

Figure 11: The model system. E and B are the electric and the magnetic components of a single electromagnetic probe field, Ω_i ($i \in \{a, b, c\}$) are Rabi frequencies of coherent coupling fields, and r is an incoherent pump field. (b) A possible realization in metastable Neon.

In the following it is shown how the dense gas approach can be used to obtain lossless negative refraction in an active, i.e., amplifying dens gas of metastable Neon atoms. A weak incoherent pumping field can be facilitated to reduce absorption or to transfer the system to an active state in a controlled fashion [53].

The model system is shown in Fig. 11; it can be realized, e.g., in metastable Neon atoms where the probe transitions have a wavelength of about $5.4\,\mu$m. E and B indicate the electric and the magnetic component of the probe field, while the Ω_i ($i \in \{a, b, c\}$) are coherent control fields. r indicates an incoherent pump rate.

The various control fields serve different purposes. It is a major problem in designing media for negative refraction that magnetic and electric dipole allowed transitions naturally are rarely degenerate. To address this problem, Ω_c is used to give rise to an AC-Stark splitting of state $|4\rangle$, such that one of the dressed states is shifted to lower energies. This allows to counter frequency differences naturally found in Neon between the electric and the magnetic probe transitions $|3\rangle \leftrightarrow |4\rangle$ and $|1\rangle \leftrightarrow |2\rangle$. Alternatively, Zeeman shifts via magnetic fields can be used, which however requires strong magnetic fields to shift both transitions into resonance. Instead of bringing the transitions in exact resonance, a two-photon transition between $|3\rangle$ and $|2\rangle$ can be induced where $|4\rangle$ only serves as virtual intermediate state. Both techniques allow to lessen the stringent requirement of near-degenerate electric- and magnetic-dipole allowed transitions to achieve negative refraction [53].

The incoherent pumping field r effectively induces a population inversion on the electric probe transition. That way, absorption in the magnetic component of the probe field can be countered by gain in the electric component of the same field. Successively increasing r allows to tune the system from passive to an active, amplifying state. This way, for the first time a controlled transition to an amplifying negative refractive media is possible.

Finally, the four state $|1\rangle$ to $|4\rangle$ are in a closed-loop configuration as discussed in Sec. 3.1. It turns out that this configuration effectively allows to increase the magnetic response by about one power of the fine structure constant α due to scattering of the electric probe field component and the control fields into the magnetic probe field mode. Since the probe field enters the multiphoton resonance condition for the given level scheme twice with opposite signs, this scattering mechanism is present for arbitrary probe field frequencies [55].

The optical response to the weak probe beam can be calculated using linear response theory. For this, the equations of motion of the system are solved up to linear order in the applied probe field. But achieving negative refraction typically requires both electric and magnetic response of the medium. Sufficient magnetic response, however, according to current knowledge is only possible for dense media, where the individual atoms cannot be treated individually. Then, local electromagnetic fields E_L experienced by the atoms are different from the externally applied fields E_E, as expressed by the Lorentz-Lorenz relation $E_L = E_E + (4\pi/3)P$. Here, P is the medium polarization. Thus, the local fields can be large if the medium polarization is large. It is important to note that local fields appear in the Hamiltonian and the equations of motion, but it is the external field which is the weak field that must be used in the linear response expansion. Still, in the literature typically the solution for density matrix is expanded to first order in the local field and only afterwards corrected by a local field correction. This approach does not give satisfactory results in our system, most likely due to a large medium polarization and this strong local fields.

Therefore, here the local fields are replaced already in the equations of motion via the Lorentz-Lorenz relations [Bow93]. This has the advantage that an expansion in the weak *external* field is possible. But the replacement renders the equations of motion non-linear since the polarization itself depends on the density matrix of the system. In order to extract the linear response coefficients, the non-linear equations of motion are solved numerically for different intensities of the probe beam which allows to obtain the coefficients using linear regression [53].

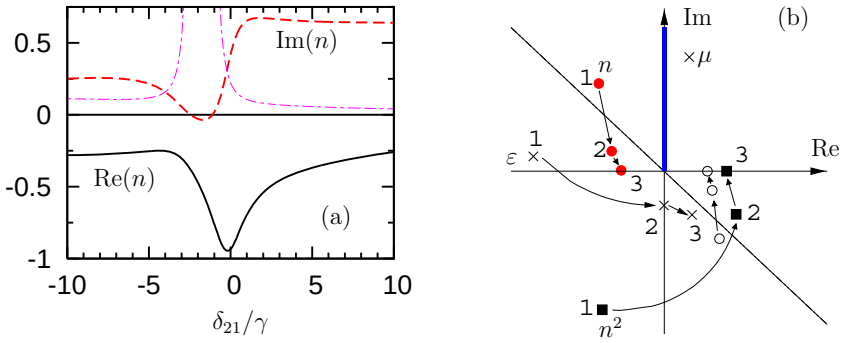

Figure 12: (a) Refractive index, absorption and figure of merit FOM = |Re(n)/Im(n)| for Neon. The parameters are $r = 1.718 \cdot 10^{-2}\gamma$, $\Omega_a = 6.3 \cdot 10^{-3}\gamma$, $\Omega_b = 5.6\gamma$, and Ω_c or magnetic fields such that the difference in the transition energies of the electric and magnetic probe field transition is 560γ. The detuning of field Ω_a is $-10^{-2}\gamma$, the gas density is $N = 2.5 \cdot 10^{17}\mathrm{cm}^{-3}$. The scaling parameter $\gamma = 10^7\mathrm{s}^{-1}$ is a typical spontaneous decay rate in metastable Neon. (b) ε, μ, $\pm n$ and n^2 as function of the incoherent pump rate. 1, 2 and 3 indicate different pump strengths.

The medium response at the probe field frequency ω_p is given by the polarization and the magnetization, which can be written as

$$\mathbf{P} = \chi_{EE}(\omega_p)\mathbf{E} + \xi_{EH}(\omega_p)\mathbf{H}/4\pi\,, \qquad \mathbf{M} = \chi_{HH}(\omega_p)\mathbf{H} + \xi_{HE}(\omega_p)\mathbf{E}/4\pi\,. \tag{8}$$

Note that the electric response depends both on the electric and the magnetic probe field component. This is unusual for atomic gases, but common, e.g., in crystals. As already mentioned, the cross-coupling allows for a considerable increase in the magnetic probe response due to scattering of control fields and the electric probe component into the magnetic probe component, if the multiphoton resonance condition is fulfilled [55]. The index of refraction is then given by [K̈07]

$$n_\pm = \sqrt{\varepsilon\mu - \frac{(\xi_{EH} + \xi_{HE})^2}{4}} \;\pm\; \frac{i}{2}\left(\xi_{HE} - \xi_{EH}\right)\,, \tag{9}$$

where the correct sign has to be chosen from physical arguments. This choice is simple for a passive system, which is necessarily absorptive, but difficult for active media, where so far no simple general criterion has been found. Fig. 12(a) shows example results for metastable Neon. The respective curves depict the refractive index, the absorption and the figure of merit, which is given by the ratio of real and imaginary part of the index of refraction.

In Fig. 12(a), results are shown for metastable neon. Negative refraction is achieved with zero absorption or even small gain, such that the figure of merit becomes very large over a frequency range of order of the natural decay rate. Thus the system enables one to study a qualitatively new parameter range not accessible with current devices, and in addition allows to significantly reduce absorption as required for a successful implementation of the interesting applications of negative refraction.

In order to choose the correct sign of the refractive index Eq. (9), the incoherent pump rate which renders the system active can be varied smoothly [53]. Then, the permeability, the permittivity and the index of refraction move in the complex plane as indicated in Fig. 12(b). Starting from the passive system, where the correct sign corresponds to the branch with absorption, the correct sign of n for the active case can be found from continuity arguments. In general, however, this procedure requires care as a simple physical interpretation of the susceptibility along the real axis in the complex frequency plane is only possible if the branch point of the square root function $n = \sqrt{\varepsilon\,\mu}$ does not lie in the upper half of the complex plane [Ska06]. This condition

is fulfilled in the present example, but was found to be violated for certain incoherent pump strengths in related systems [55].

4 Strong field light scattering off of regular structures

In atomic and molecular physics, light scattered by a quantum system is one of the primary observables used to analyze the properties of the object under study. A systematic characterization of the light is possible with the help of the different correlation functions of light [Gla07].

Physics related to the first-order correlation function already played a major role in the early days of quantum physics. For example, Young's double slit together with different extensions frequently served as thought experiment in discussions on the foundations of quantum mechanics. A modern variant of Young's experiment involves light scattering off of atoms [Eic93b, Esc01]. As in the original setup, light is scattered such that different indistinguishable pathways connect source and detector, and thus interference may arise. The most direct analogy to the double slit experiment is achieved for a structure of different atoms, but analogous interference is also possible with single particles, where the different interfering pathways correspond to different internal time evolutions as discussed in Sec. 2.1 [Lin05b] [29].

There is, however, a difference between the classic double slit setup and the corresponding realizations with light scattered by atoms. The atoms have internal structure, and their scattering properties depend on the intensity of the scattered light. In the limit of very small light intensity, the scattered light is almost entirely coherent, such that high interference visibility is possible. For strong driving fields, however, the atomic transitions saturate, and the interference visibility vanishes [Sko01]. Yet, most applications would benefit from a high intensity of coherently scattered light.

This motivates the study of quantum interference in light scattered by regular structures driven by strong laser fields [32]. As a starting point, a pair of distinguishable atoms located at positions $\vec{r}_a$, $\vec{r}_b$ and separated by $\vec{r}_{ab}$, is studied. The particles are assumed to be two-level atoms with transition frequency ω_0. The driving laser field has frequency $\omega_L = ck_L$, wave vector $\vec{k}_L$, and is aligned such that $\vec{k}_L \cdot \vec{r}_{ab} = 0$ (see Fig. 13). The distance of the particles is assumed large enough such that direct interactions between the particles can be neglected.

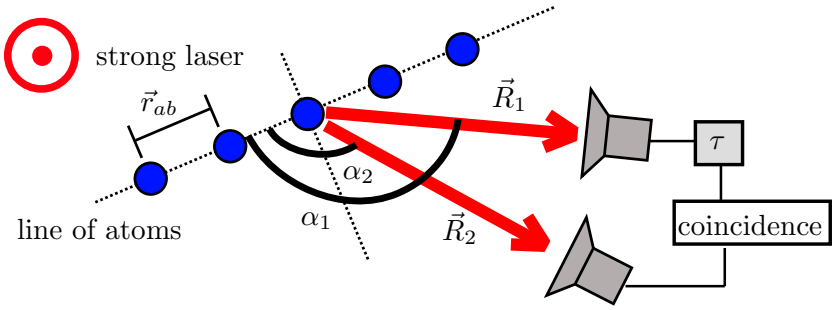

Figure 13: Two-level atoms positioned in a linear structure with constant inter-particle distances $\vec{r}_{ab}$. All atoms are driven by a near-resonant strong laser field with wave vector $\vec{k}_L$. Two detectors D_1, D_2 placed in observation directions $\vec{R}_1, \vec{R}_2$ measure properties of the emitted scattered light such as intensity, spectrum, and correlations between different photons. τ depicts a delay unit for the coincidence measurements. The observation directions are also characterized by the angles α_1, α_2 between $\vec{r}_{ab}$ and $\vec{R}_1, \vec{R}_2$. The atoms and the detectors are located in a plane, and the driving field propagates perpendicular to this plane.

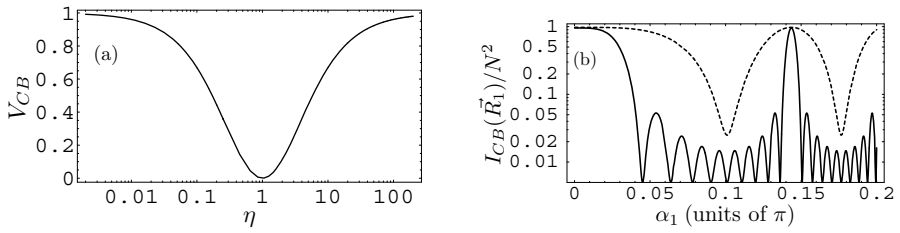

Figure 14: (a) Central band visibility V_{CB} as function of η for a resonant strong driving field. (b) Central band intensity $I_{CB}(\vec{R}_1)/N^2$ (arbitrary units) as function of α_1. Here, the bath parameters are such that $V_{CB} = 0.95$. Solid line: $N = 10$, dashed curve: $N = 2$. Note the different axis scales of the two subfigures.

In the limit of a strong driving field, the spectrum of the scattered light separates into distinct spectral bands like in the well-known single-atom Mollow resonance fluorescence spectrum [Scu97], such that spectral properties have to be defined for each spectral band separately. It is found that the scattered light separates into a central spectral band at the laser frequency ω_L (C), and two left/right sidebands (L, R) at frequencies $\omega_\pm$ centered around ω_L.

As the key element of the control scheme, in the following, it is assumed that the atoms are embedded in a frequency-dependent environmental bath, such that the mode densities at the two sideband frequencies ω_+ and ω_- differ considerably. Thus, the structure interacts with different mode densities at the various dressed-state frequencies. Because the spontaneous decay rates $\gamma(\omega)$ are proportional to the density of modes at the transition frequencies, the dressed-state populations redistribute depending on the parameter $\eta = \gamma(\omega_+)/\gamma(\omega_-)$. Techniques to achieve such a modification of the vacuum were demonstrated experimentally, e.g., in [Zhu88, Flo04].

4.1 First-order correlation function: Interference recovery

For the measurement of the first-order correlation function or intensity of the scattered light, a single detector at a position given by the angle α (see Fig. 13) registers the light intensity at a particular frequency in the optical far-field limit. As observable, the intensity of the central spectral band is chosen, for which the visibility

$$V = \frac{I_{max} - I_{min}}{I_{max} + I_{min}}$$

is defined, where I_{max} $[I_{min}]$ are the maximum [minimum] intensity as a function of the detector position α. The driving field is assumed to be on resonance and strong. Then, for plain vacuum with $\eta = 1$, the visibility is found to be zero.

This conclusion changes completely if the surrounding electromagnetic reservoir is modified, see Fig. 14(a). It can be seen that maximum visibility ($V \approx 1$) can be obtained for $\eta \ll 1$ or $\eta \gg 1$. The case $\eta \to 0$ is achieved if the mode density at the low-frequency sideband is much larger than the corresponding high-frequency sideband mode density, or if the high-frequency sideband mode density vanishes. The opposite case $\eta \to \infty$ is achieved if the conditions for the densities at high- and low-frequency sideband are interchanged. Thus, if the densities of the electromagnetic field modes at the dressed transition frequencies $\omega_\pm$ differ considerably, then the interference pattern is recovered in the central band with near-complete visibility. This opens the possibility to explore coherent light scattering in the limit of strong driving fields [32]. Figure 14(b) shows a corresponding interference pattern versus detection angle α.

The interpretation for this recovery can be given in terms of scattering via symmetric and anti-symmetric collective states of the two-atom system [32]. Note that this collective symmetry property is independent of the single-particle dressed states, which

can be either symmetric or anti-symmetric. As shown in [Sko01], transitions involving symmetric collective states give rise to interference with a bright center. This means that the light intensity is at a maximum value if the path lengths from the atoms to the detector are the same. Scattering via the anti-symmetric state leads to the opposite dark-center interference. In plain vacuum at strong driving, both scattering channels have equal probability, such that the two kinds of interference cancel each other. In a modified vacuum surrounding, for $\eta \ll 1$ or $\eta \gg 1$, however, only symmetric collective states are populated. Thus one finds bright center interference, as can also be seen from Fig. 14(b).

The discussion of the first-order correlation function can be extended to many-atom ensembles. If N independent two-level atoms are uniformly distributed in a linear chain ($r_{ab} = r_{i,i-1}$), then their central-band intensity (up to a pre-factor) evaluates to

$$I_{CB}(\vec{R}_1) = N(1-z) + z\mathcal{F}(\delta_1)\,. \tag{10}$$

Here, $\delta_i = k_L r_{ab}\cos\alpha_i$, $\mathcal{F}(x) = \sin^2[Nx/2]/\sin^2[x/2]$, and z is a function of the dressed state populations. Maxima of the light intensity I_{CB} scattered into the central frequency band occur for $k_L r_{ab}\cos\alpha = 2\pi n$ with $z = 1$, where the intensity $I_{CB}^{(max)}(\vec{R})$ scales with the number of atoms N squared. Thus the central-band visibility is significantly improved. In analogy to the multi-slip experiment in classical optics, the resolution of the sub-wavelength pattern of the different maxima scales with the atom number, see Fig. 14(b).

4.2 Second-order correlation function: Lithography

In this section, the second-order correlation function of the steady-state resonance fluorescence emitted in the three spectral bands is discussed. The coherence properties of an electromagnetic field, at space-point $\vec{R}$, can be evaluated with the help of the second-order coherence functions:

$$g^{(2)}_{mn}(\tau,\vec{R}_1,\vec{R}_2) = \frac{\langle a_m^+(t,\vec{R}_1)\, a_n^+(t+\tau,\vec{R}_2)\, a_n(t+\tau,\vec{R}_2)\, a_m(t,\vec{R}_1)\rangle}{\langle a_m^+(t,\vec{R}_1)\, a_m(t,\vec{R}_1)\rangle\, \langle a_n^+(t,\vec{R}_2)\, a_n(t,\vec{R}_2)\rangle}, \tag{11}$$

where a_n^+ (a_n) ($n \in \{C,L,R\}$) are the photon creation (annihilation) operator for the central (C) spectral band or the sideband modes (L,R) which occur at strong driving. The quantity $g^{(2)}_{mn}(\tau)$ can be interpreted as a measure for the probability for detecting one photon emitted in mode m and another photon emitted in mode n with delay τ. From now on, all correlation functions are evaluated for $\tau = 0$, and the variable τ is dropped. For $\tau = 0$, the second-order correlation function determines the photon statistics of the emitted light, which could, e.g., be (sub-) poissonian, or coherent. Further, the two Cauchy-Schwarz parameters

$$\chi_L(\vec{R}_1,\vec{R}_2) = \frac{g^{(2)}_{LL}(\vec{R}_1,\vec{R}_2) g^{(2)}_{RR}(\vec{R}_1,\vec{R}_2)}{[g^{(2)}_{LR}(\vec{R}_1,R_2)]^2}\,, \tag{12a}$$

$$\chi_R(\vec{R}_1,\vec{R}_2) = \frac{g^{(2)}_{LL}(\vec{R}_1,\vec{R}_2) g^{(2)}_{RR}(\vec{R}_1,\vec{R}_2)}{[g^{(2)}_{RL}(\vec{R}_1,R_2)]^2}\,, \tag{12b}$$

relate the correlation between photons emitted into individual modes to the cross-correlation between photons emitted into two different modes. If $\chi_L < 1$ or $\chi_R < 1$, then respective Cauchy-Schwarz inequalities are violated, and the correlations are non-classical [Lou80].

To evaluate potential applications in lithography, the setup is specialized to the case of a medium sensitive to two-photon exposure [Bot00, D'A01, Xio05, Hem06] [49]. For this, both photons are assumed to be detected at the same position $\delta = kr_{ab}\cos(\alpha)$, i.e. $\vec{R}_1 = \vec{R}_2 \equiv \vec{R}$. A suitable performance indicator for lithography is the interference

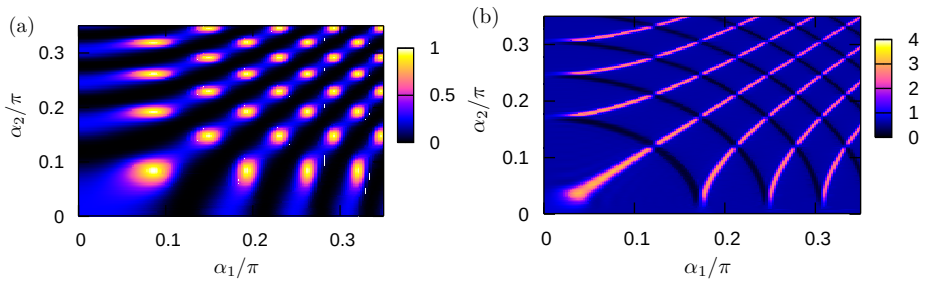

Figure 15: The Cauchy-Schwarz parameter $\chi_L = \chi_R$ as function of detector positions α_1, α_2. Here, $r_{ab}/\lambda = 7$. The number of atoms is (a) $N = 2$ and (b) $N = 10$.

fringe resolution, which is a measure for the smallest structure size that can be created by means of optical exposure via such a system. In the strong-field limit, with resonant driving field, one finds $g^{(2)}_{CC}(\vec{R}) = 1 + \cos^2\delta$. Comparing this result to the weak driving field case, where the different spectral bands are unresolved [Sko01], it is found that the spatial fringe resolution is twice as high in the strong field case as in the weak field case. Thus, simply increasing the driving field strength effectively doubles the resolution of the spatial pattern around the central frequency ω_L [32].

More insight in the system properties can be gained by studying light emitted into the spectral sidebands (L, R) [52]. Again, detection in the far zone limit is assumed, but this time with detectors at different positions. For this setup, the Cauchy-Schwarz parameters in Eq. (12) turn out to be equal $\chi_L = \chi_R$, and are shown in Fig. 15(a) for an inter-particle distance $r_{ab} = 7\lambda$ and for two atoms ($N = 2$). It can be seen that the Cauchy-Schwarz inequalities are violated for broad ranges of detector positions δ_1, δ_2, where $\chi_L = \chi_R < 1$. The structure of χ_L and χ_R can be understood by inspecting Eq. (12). The Cauchy-Schwarz parameters are given by the ratio of the product of the sideband second-order photon correlations $g^{(2)}_{LL}(\vec{R})$ and $g^{(2)}_{RR}(\vec{R})$ to the cross correlation $g^{(2)}_{LR}(\vec{R})$ or $g^{(2)}_{RL}(\vec{R})$ squared. Therefore, the oscillatory structures of both quantities combine to give the result in Fig. 15(a). It is interesting to note that it is not possible to distinguish whether the first photon is emitted on the left or on the right sideband, since the two different cross-correlations $g^{(2)}_{LR}(\vec{R})$ and $g^{(2)}_{RL}(\vec{R})$ are equal.

These results can also be generalized to the case of N independent two-level atoms that are uniformly distributed in a regular chain with inter-particle distance r_0. Consistent with our assumption of detection in the far-zone limit, the linear dimension of the chain $L = (N-1)r_0$ is much smaller than the distances between chain and detectors $|\vec{R}_1|$ and $|\vec{R}_2|$. An example for $N = 10$ atoms is shown in Figure 15(b). In this figure, the Cauchy-Schwarz parameters range between below unity up to four.

5 Collective quantum dynamics in ensembles of atoms

If two atoms are close to each other, they can interact via the vacuum radiation field in a process where a (virtual) photon emitted by one of the atoms is re-absorbed by the other atom [Aga74]. This dipole-dipole coupling gives rise to a collective quantum dynamics, which can significantly deviate from a corresponding single-particle dynamics. In the following, two different approaches are presented to deal with such collective systems. The first approach in Sec. 5.1 takes into account the exact position-dependent coupling of the individual particles to the relevant electromagnetic fields. This enables one to study in particular the geometrical structure of the inter-particle coupling, but the computational complexity restricts the treatment to few-particle systems. The second approach employed in Sec. 5.2, on the other hand, neglects the individual positions of the particles by assuming that all particles interact with the external fields

in the same way. This approximation was introduced by Dicke [Dic54], and allows to analytically treat systems of arbitrary particle number. However, within this approximation the notion of an individual particle looses its meaning and the precise structure of the inter-particle coupling cannot be studied. Thus both approaches are complementary.

5.1 Geometrical structure of the dipole-dipole interaction

Most previous work in quantum optics on dipole-dipole interacting atoms has focussed on two-level systems, often restricted to somewhat special geometries. For example, the alignment of the transition dipole moments, the interatomic distance vectors, the laser field wave vectors and the observation direction are often assumed fixed and parallel or perpendicular to each other [Fic02]. The motivation for this might be that for collective effects to occur, the emitting and the absorbing transitions should be near-degenerate, and the polarization of the emitted photon must match the absorbing transition dipole moment. Thus often this dipole-dipole interaction is thought to couple only non-orthogonal transition dipole moments. This restriction is in complete analogy to the stringent conditions for the appearance of spontaneous-emission interference between transitions in single-particle systems, which only occurs for non-orthogonal transition dipole moments, as discussed in Sec. 2.1 [Fic05].

It turns out, however, that in contrast to the single-atom case, dipole-dipole couplings are also possible between transitions with orthogonal dipole moments [Aga01] [31, 41, 43]. Effects of such orthogonal couplings have been observed, for example, in low-dimensional samples of ultracold gases [Car04]. Simply speaking, this occurs if the projection of the polarization of the emitted photon on the absorbing dipole moment is non-zero, a condition which strongly depends on the geometry of the setup [31]. In the following, implications of these dipole-dipole couplings between orthogonal transition dipole moments (DDOTDM) are discussed [31, 41, 43].

5.1.1 Geometry-dependent dynamics via vacuum-induced coherences

As a first step, it is shown that the DDOTDM couplings may lead to a geometry-dependence of the electronic dynamics for a pair of laser-driven Λ-type atoms, see Fig. 16 [31]. The two atoms are driven by two laser fields propagating in z direction, and the total fluorescence intensity of the light scattered in y direction is recorded. The first atom is located in the coordinate system origin, the second atom is located at $\vec{r}_{12}$. In Fig. 17, the fluorescence intensity emitted in y-direction is shown for two different geometries $\vec{r}_{12}$. In the first case, both atoms are aligned along the z axis. In the second case, the second atom is in the $x-y$ plane. In both cases, the remaining setup of driving fields and detectors is the same.

From Fig. 17, it is found that the spatial orientation of the two-atom pair alone can decide if the system reaches a true constant steady state or if it exhibits periodic

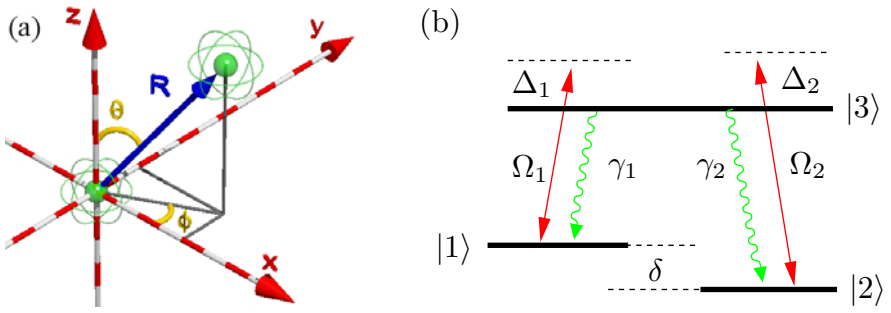

Figure 16: (a) System of two dipole-dipole interacting atoms in arbitrary geometry. (b) Atomic level structure as used in Sec. 5.1.1

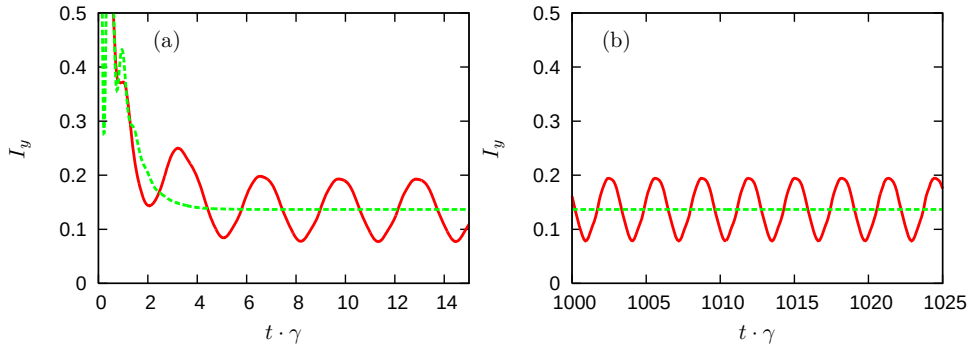

Figure 17: (a) Short time and (b) long time dynamics of the fluorescence light emitted in y-direction. The two atoms are three-level Λ-type atoms, where each of the two dipole-allowed transition is driven by a stationary laser field ($\Omega_1 = \Omega_2 = 5\,\gamma$, $\Delta_1 = 0$, $\Delta_2 = 2\,\gamma$). The geometry is chosen as $\phi = \pi/4$, and $\theta = \pi/2$ (solid red line) and $\theta = 0$ (dashed green line). Since the oscillation of the solid line continues undamped for all times. Apart from the angle θ, all parameters for the two curves are identical.

oscillations in the long-time limit. If the two atoms are aligned along the z axis, then the system reaches a steady state (green curve). If, however, atom B is in the $x-y$ plane, then the system never reaches a steady state, and the intensity exhibits periodic oscillations in the long-time limit, see the red curve in Fig 17(b).

This unusual geometry dependence of the internal dynamics can directly be related to the DDOTDM. For the case where the system reaches a steady state, the DDOTDM vanish. But for the case where the system exhibits periodic oscillations in the emitted light intensity, the DDOTDM couple the dipole-allowed transitions with orthogonal dipole moments in the two atoms. Then, each transition is effectively driven twice. First, the direct driving by the external laser field with frequency of the first laser field. Second, indirect driving via the DDOTDM with frequency of the second driving field. Thus, if the two laser field frequencies differ, the DDOTDM effectively give rise to a bichromatic driving of the atoms, which leads to the non-stationary long time limit.

Thus, it is found that the DDOTDM couplings enable one to influence the dynamics of a pair of atoms simply by changing the relative orientation of the two atoms, such that the evolution strongly depends on the system geometry.

5.1.2 Orthogonal dipole-dipole couplings in time-dependent geometries

The DDOTDM strongly depend on the relative orientation and distance of the involved particles. In many situations of interest, however, this geometry is not fixed. For example, in a linear trap, the inter-atomic distance usually can be described classically as a sinusoidal oscillation around a mean distance. In this case, a dependence of the dynamics on the orientation of the dipole moments relative to the oscillation direction can be expected. A gas of atoms corresponds to a setup where both the orientation and the distance of any given pair of atoms changes with time. Thus the question arises, whether the geometry-dependent effects of the dipole-dipole interaction of orthogonal transition dipole moments (DDOTDM) survive an averaging over different geometries [48]. A convenient observable to find an answer to this question is the oscillation of the fluorescence intensity in the long time limit found in the previous Sec. 5.1.1, which could be traced back exclusively to the DDOTDM.

Two different ansatzes for an averaging of the configuration space are compared. First, one can assume that the internal electronic dynamics is much faster than the change of the geometrical setup [adiabatic case (AC)]. In the opposite limit, the change in geometry is fast enough such that the atoms essentially see an averaged interaction potential [average potential (AP) method]. The latter approach for example is used

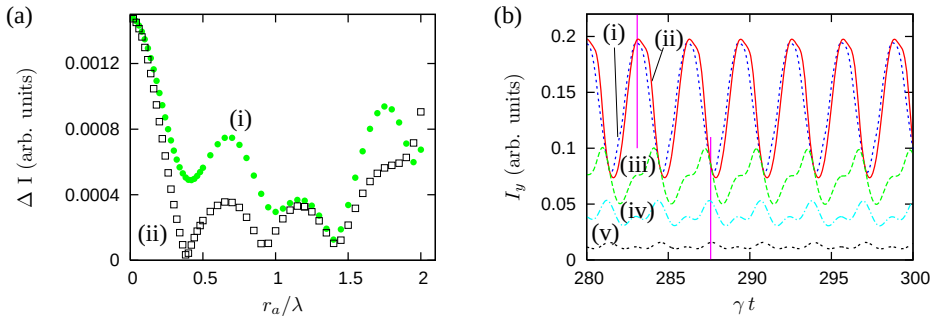

Figure 18: (a) Dependence of the amplitude of the fluorescence intensity modulations on the oscillation amplitude r_{12} of the atom for a mean distance $r_m = 2.25\lambda$. In (i) the AC is used and in (ii) the AP method. The inter-atomic distance vector is oriented such that $\phi = \pi/4$ and $\theta = \pi/2$. The laser parameters are $\Omega_1 = 3\,\gamma$, $\Omega_2 = 5\,\gamma$, $\Delta_1 = 0$, $\Delta_2 = 2\gamma$, and the two lower states are assumed degenerate $\delta = 0$. (b) Time-dependent fluorescence signal for different fixed distances r_{12} without any averaging. (i) $r_{12} = 0.10\,\lambda$, (ii) $r_{12} = 0.08\,\lambda$, (iii) $r_{12} = 0.06\,\lambda$, (iv) $r_{12} = 0.05\,\lambda$, (v) $r_{12} = 0.04\,\lambda$. The other parameters are as in (a). The vertical lines allow to easily judge the relative phase shifts of the different curves.

in the context of ultracold quantum gases to derive the $1/r$ long-range potential from the dipole-dipole coupling of parallel dipole moments by averaging over all possible orientations of the inter-atomic distance vectors [Cra84].

Averaging over different parameter ranges of relevance, it is found that in general the orthogonal couplings can survive an extensive averaging over different geometries as long as the inter-particle distance remains small [48]. The magnitude of the effects in the averaged signal, however, strongly depends on the averaging range, and also on the averaging method. Typically, one- or two-dimensional systems can be expected to show larger effects of the dipole-dipole coupling. Also, the two averaging methods considered can give very different results when averaged over the same set of geometries. In most situations, however, the case where the change in geometry is slow as compared to the internal dynamics is more favorable.

An example for the averaged results, in Fig. 18 results are shown for a sinusoidal oscillation of the inter-particle distance r_{12} around a mean value,

$$r_{12}(\alpha) = r_m + r_a\, \sin(\alpha)\,.$$

In Fig. 18(a), the fluorescence intensity oscillation amplitude in the long-time limit ΔI is shown against the oscillation amplitude r_a for a mean distance $r_m = 2.25\lambda$. It can be seen that the curve exhibits a series of resonances, which occur due to an alternating destructive and constructive superposition of the contributions from different distances in the averaging process. This can be seen from Fig. 18(b), where some examples of unaveraged time-dependent signals for small inter-atomic distances are shown. For distances larger than about $0.06\,\lambda$, the relevant contributions oscillate approximately in phase, see curves (i) and (ii). For smaller distances, however, the contributions move out of phase, as can be seen from curves (iii)-(v). Curves (iv) and (v) approximately have maxima where curves (i) and (ii) have minima, and vice versa. Curve (iii) is an intermediate case. Therefore, the oscillations with different phases cancel each other in the averaging process if distances below about $0.06\,\lambda$ are included in the averaging. Similar relative phase shifts of the intensity modulations occur also for larger inter-particle distances.

In Fig. 18(b), at very small distances, the fluorescence intensity decreases, because then the level shifts induced by the dipole-dipole coupling are strong enough to shift the relevant transition frequencies out of resonance with the driving laser fields.

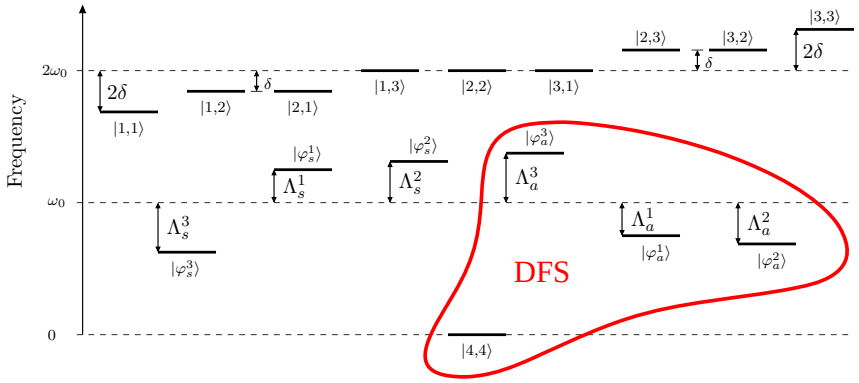

Figure 19: Collective state space of two interacting 4-level atoms. The excited states are Zeeman split and both atoms are located in the $x-y$ plane. The lowest state corresponds to both atoms in the ground state. In the intermediate state manifold, one atom is excited, whereas the other is not. In the upper set of states, both atoms are in one of the three excited states. The red curve indicates the four-dimensional decoherence free subspace.

The approximate minimum in curve (ii) of Fig. 18(a) is due to the fact that for this oscillation amplitude, the DDOTDM are small at the classical turning point of the oscillation, such that the influence of the DDOTDM are small. Clearly, the two averaging methods corresponding to different physical situations give very different results for this set of parameters.

Other situations of interest are studied in [48], such as averaging over the orientation, over orientation and interparticle distance, and over particle A flying past particle B on a straight trajectory.

5.1.3 Breakdown of the few-level approximation in collective systems

From the above discussion it is clear that the DDOTDM in general play a crucial role in the collective dynamics of dipole-dipole-interacting systems. In particular, one has to realize that DDOTDM may lead to a population transfer to excited states that are not driven by any external field [Aga01] [41]. To understand the effect of this for collective systems rigorously, it is useful to study the archetype case of two dipole-dipole interacting atoms, and model each atom by complete sets of angular momentum multiplets. As a first step, the intuitive result can be proven that the dipole-dipole induced energy shifts between collective two-atom states are invariant under rotations of the separation vector if complete and degenerate multiplets are considered[41]. The physical reason for this is that such a system does not have a preferred direction in space.

This result, however, can only be established if the DDOTDM are included in the analysis, and if complete angular momentum multiplets are considered. On the contrary, the artificial omission of any of the Zeeman sublevels of a multiplet leads to a spurious dependence of the energy shifts on the orientation, and thus to incorrect predictions. For example, if only one excited state $|e\rangle$ and the ground state $|g\rangle$ are retained, the position-dependent energy splitting between the entangled two-particle states $(|e,g\rangle \pm |g,e\rangle)/\sqrt{2}$ is recovered which has previously been reported for a pair of two-level systems.

Thus the few-level approximation violates the expected rotational invariance, and one has to conclude that in general the few-level approximation which is ubiquitous in quantum optics cannot be applied to collective systems. A state reduction of the angular momentum multiplets is only possible for few selected geometries, which can easily be identified using the techniques developed throughout the analysis in [41].

5.1.4 Multi-particle decoherence free subspaces

In the previous Sec. 5.1.3 it was explained that the DDOTDM enforce the inclusion of complete angular momentum multiplets in modelling dipole-dipole interacting systems. On the one hand, this renders the analysis more demanding as compared to the treatment of interacting two-level systems because of the larger state space. On the other hand, however, multilevel systems offer interesting perspectives for novel applications. One example is the possibility for a decoherence-free subspace (DFS) [Zan97, Lid98] in a system of two dipole-dipole interacting multi-level atoms [43] The ground state of each atom is taken to be a S_0 singlet state, and the excited state multiplet is a P_1 triplet. A subspace $\mathcal{V}$ of the complete Hilbert space is called decoherence-free if the time evolution inside $\mathcal{V}$ is purely unitary. An analysis of the system dynamics reveals that in the limit of vanishing interatomic distance, the state space of our system contains a four-dimensional DFS, see Fig. 19. The excited states in the DFS are the generalization of the well-known sub-radiant Dicke state found in two two-level systems. Their lifetime and thus the operation time of the DFS depends on the interatomic distance, and becomes infinite in the limit of vanishing interatomic distance. Using a single cw laser field, the DFS can be populated probabilistically without requiring, e.g., field gradients on the wavelength distance scale as employed by previously proposed schemes. After preparing the system in the DFS, arbitrary single-qubit operations can be executed between two excited states within the DFS either using a static magnetic field or a rf field. Thus it is possible to induce a controlled dynamics within a subspace that is approximately decoupled from the dissipative interaction with the vacuum field. It should be noted that despite the approximate spontaneous emission suppression, the lifetime of such a system is typically short as compared to coherence times of nuclear spin systems. But the operation times can be significantly shorter than in spin systems due to the large atom-field coupling constants, such that the number of operations per coherence time may become comparable. The antisymmetric sub-radiant states can also be identified as long-lived entangled states.

5.2 Many-particle quantum dynamics

In the Dicke model employed in this section, the different constituents of the ensemble are assumed to be confined to a small region in space such that the relevant electromagnetic field modes interact with all atoms in the same way, see Fig. 20(a). In view of most experiments done so far, for example in extended gas cells, the validity of this approximation is not obvious. Indeed, extended media show additional effects like a re-absorption of emitted light that are not captured by the original model by Dicke. Nevertheless, the Dicke model allows to successfully predict the relevant features of the collective quantum dynamics. More recent experiments allow to closely approximate

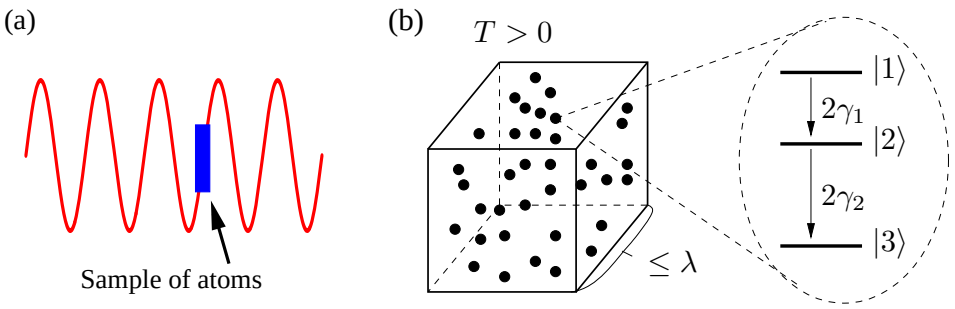

Figure 20: (a) Schematic illustration of the Dicke approximation. The atoms are concentrated in a region in space which is small as compared to the wavelength of the relevant electromagnetic fields. (b) Setup with three-level atoms in ladder configuration in a thermal bath with temperature $T > 0$ as used in Sec. 5.2.2.

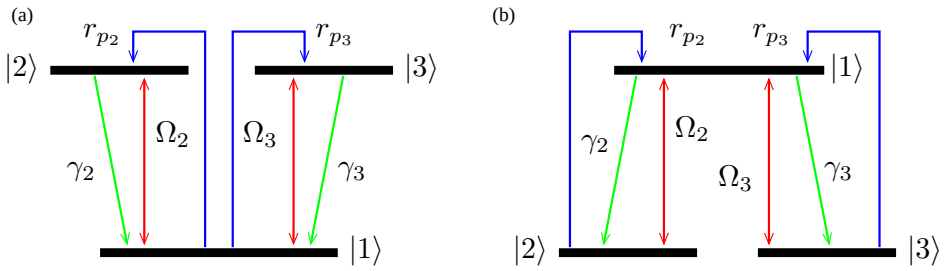

Figure 21: Three-level atoms in (a) V- and (b) Λ configuration. Red arrows indicate coherent driving, green arrows spontaneous emission, and blue arrows incoherent pumping.

the original conditions assumed by Dicke [Gre00]. If Fig. 20(b), a setup with a small sample of atoms together with the internal structure that will be analyzed in Sec. 5.2.2 is shown as an example.

In essence, the small sample approximation allows to introduce collective operators, which are sums over single-particle operators. These enable one to solve the collective Master equation in certain limiting cases analytically for arbitrary particle numbers. But it also entails conceptional differences to the analysis in Sec. 5.1. In the Dicke limit, e.g., it is only possible to evaluate how many of the atoms are excited, but not which of the atoms. Thus the notion of an individual particle looses its meaning in this framework.

5.2.1 Coherent control of collective quantum dynamics

Collective quantum systems are known to offer a number of interesting properties, such as an accelerated internal evolution, or a certain robustness against perturbations [Dic54]. In previous studies, the implications of collectivity have been analyzed in great detail, but the focus was mostly on a description of the properties [And93]. In contrast, for most applications, a precise control of the system under study is required. For example, a complete and rapid transfer of the system population between various system states may be desirable in order to control the optical properties of the system. Thus it is not surprising that many control schemes have been proposed, though mostly for single-atom systems [Fic05]. In the following, the question is addressed whether similar control schemes can also be found for for collective quantum systems [6, 10, 13, 19, 23, 44].

As model system, ensembles of three-level atoms in V- or Λ configuration are studied, see Fig. 21. The atoms are embedded in a mode-selective cavity, which induces quantum interference between the two dipole-allowed transitions [Pat99, Zho00]. This interference renders the systems sensitive to the relative phase Φ of the two coherent driving fields, which can thus be used as a control parameter [c.f. Sec. 2.2]. The coherent fields are taken to be strong, such that an analysis in terms of the dressed states of the system is convenient. In the following, the population of one of these dressed states,

$$|\Psi_1\rangle \quad = \quad \frac{\Omega_3}{\Omega}|2\rangle - \frac{\Omega_2}{\Omega}|3\rangle, \qquad \Omega = \sqrt{\Omega_2^2 + \Omega_3^2}, \tag{13}$$

will be used as an observable. This dressed state is a linear combination of the two excited states in the V-type system, and of the two ground states in the Λ-type setup. In addition, the total fluorescence intensity emitted on the two dipole-allowed transitions is studied.

Fig. 22(a) shows the steady-state population in the collective dressed state $|\Psi_1\rangle$ per atom of the V-type system for different numbers of atoms N versus the relative phase $\Delta\phi$ between the two applied strong resonant laser fields. For a single atom

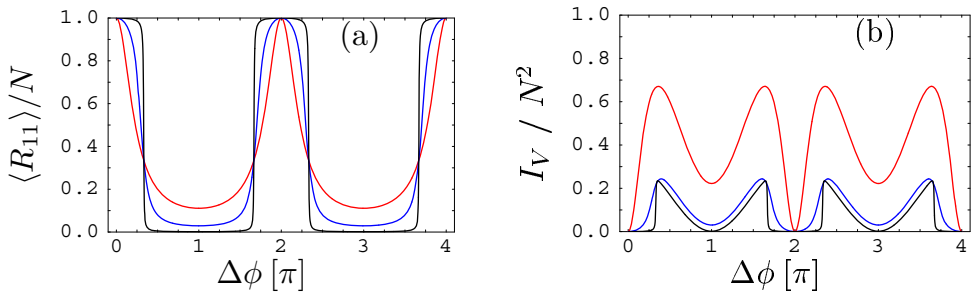

Figure 22: (a) Population of one of the dressed states for different number of atoms in the ensemble plotted against the relative phase ϕ of the driving fields. (b) Fluorescence intensity emitted by the ensemble. In both cases, the driving fields are strong, and the red line corresponds to number of atoms $N = 1$, the blue line to $N = 10$, and the black line to $N = 200$. Further $\Omega_2 = \Omega_3$, $\eta = 1$, $\Phi(r) = 1$ and $\mathcal{C} = 2$.

($N = 1$), the atom may only be trapped in $|\Psi_1\rangle$ for $\Delta\phi = n \cdot 2\pi$ ($n \in \{0, 1, \dots\}$). With increasing number of atoms, the range $\delta(\Delta\phi)$, for which the collective coherent population trapping effect occurs, grows until in the limit $N \to \infty$ the system exhibits jumps between two states with either all or none of the population in the collective state $|\Psi_1\rangle$. Increasing the number of atoms involved also can be shown to lead to a more rapid transfer of the atoms into the trapping states or vice versa. These properties may be used to build fast optical switching devices conveniently controlled by the relative phase of the two laser fields. The steady state of the collection of atoms also influences the absorption or gain of an additional weak probe beam, such that the fast switching between the ground and the excited state might be used to construct e.g. a quantum optical transistor.

The collective steady-state fluorescence intensity per emitted atom I_V/N^2 with minima $\Delta\phi = \pi n$ for $n \in \{0, 1, 2, \dots\}$ is depicted in Fig. 22(b). A comparison with Fig. 22(a) shows that the minima occurring for even n are due to the trapping of the population in the collective dressed state $|\Psi_1\rangle$, i.e. in the collective upper bare states $|2\rangle$ and $|3\rangle$. While for the single atom case the intensity only vanishes exactly at $\Delta\phi = 2\pi n$, the trapping range increases with the atom number as discussed for the populations. In Fig. 22(b), at phase differences corresponding to odd n, the fluorescent intensity also tends to zero for $N \gg 1$. However, at these phase differences the population is not trapped in $|\Psi_1\rangle$ as for even n, but with equal weights in the two other dressed states. This means that 0.5 of the atomic population is in the ground bare state $|1\rangle$, while 0.25 of the population is in each of the upper bare state $|2\rangle$ and $|3\rangle$. As the inhibition of fluorescence does not occur in the single atom case, these minima may be associated with subradiant states: The photons emitted by the half of atoms in the excited states is absorbed by the other half in the ground state.

Similar results are found for the Λ-type system [6, 19]. It was further shown that also other control parameters allow to prepare the systems favorably, e.g., incoherent pump fields [10] or thermal baths [13]. The localization of small ensembles of atoms is discussed in Sec. 6.1.2 of this work.

5.2.2 Quantum correlations via an incoherent bath

Entanglement and correlations are key resources for applications in quantum information processing. A major challenge in this area typically is the preservation of these correlations under perturbing interactions with the environment that cause decoherence. But surprisingly, it has been shown that under certain conditions the interaction with an incoherent heat bath can be favorable and even induce correlations [Arn01, Ple02]. In this Section, it will be shown that this favorable impact also can be observed for small ensembles of atoms subject to an incoherent bath [23].

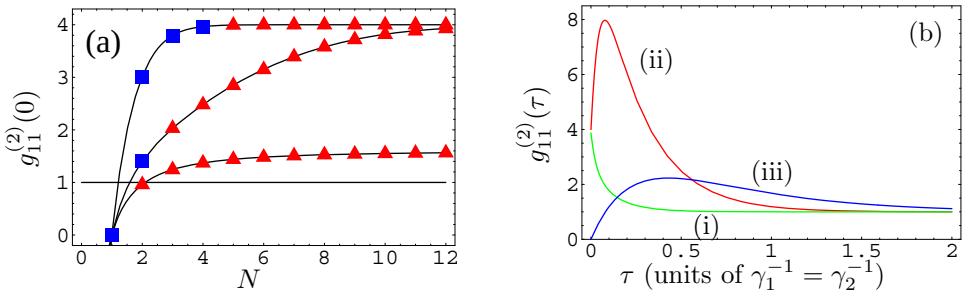

Figure 23: Second order correlation function of photons emitted on transition $|1\rangle \leftrightarrow |2\rangle$ as a function of the number of atoms in the ensemble. (a) Results for $g_{11}^{(2)}(0)$ indicating the photon statistics. The three curves correspond to different bath temperatures $\eta_1 = \eta_2 = 1$ (lower curve), 0.5, 0.1 (upper curve). In addition, red triangles (blue squares) denote bunching (anti-bunching) obtained from $g_{11}^{(2)}(\tau)$. (b) Dependence of $g_{11}^{(2)}(\tau)$ on the delay τ. (i) $N = 15$, $\eta_1 = \eta_2 = 0.6$, (ii) $N = 6, \eta_1 = 0.8, \eta_2 = 0.05$, (iii) $N = 1, \eta_1 = \eta_2 = 0.2$.

A collection of three-level atoms in ladder configuration is embedded in an incoherent bath that drives the two transitions, as shown in Fig. 20(b). The incoherent bath can either be thermal with a Boltzmann distribution of the bath excitation (for example in the microwave frequency regime), or pseudo-thermal induced by an incoherent driving field (e.g. at optical frequencies). The bath temperature can be parameterized via the parameters $\eta_i = \bar{n}_i/(1+\bar{n}_i)$, where $\bar{n}_i$ is the mean thermal photon number at the transition frequency of transition i ($i \in \{1,2\}$). Zero temperature corresponds to $\eta_i = 0$, while for hot bathes this parameter approaches unity.

The created correlations can most conveniently be measured via the light emitted by the ensemble, characterized by the normalized steady-state second order correlation function

$$g_{ij}^{(2)}(\tau) = \frac{\langle S_i^+(t) S_j^+(t+\tau) S_j^-(t+\tau) S_i^-(t)\rangle}{\langle S_i^+(t) S_i^-(t)\rangle \, S_j^+(t) S_j^-(t)\rangle}\Big|_{t\to\infty}.$$

Here, $i,j \in \{1,2\}$ parameterize the two transitions and $S_i^{\pm}$ is the atomic raising (lowering) operator on transition i. The quantity $g_{ij}^{(2)}(\tau)$ can be interpreted as a measure for the probability for detecting one photon emitted on transition i and another photon emitted on transition j with time delay τ. $g_{ij}^{(2)}(0) < 1$ characterizes sub-poissonian, $g_{ij}^{(2)}(0) > 1$ super-poissonian, and $g_{ij}^{(2)}(0) = 1$ poissonian photon statistics. $g_{ij}^{(2)}(\tau) > g_{ij}^{(2)}(0)$ is the condition for photon anti-bunching, whereas $g_{ij}^{(2)}(\tau) < g_{ij}^{(2)}(0)$ means bunching. Correlation functions with $i = j$ describe the photon statistics of the fluorescence light emitted on a single atomic transition, and $g_{i\neq j}^{(2)}(0)$ the cross-correlations between the photon emission on two different transitions.

Example results are shown in Fig. 23(a). Here, the second order correlation function at $\tau = 0$ of fluorescence light emitted on transition $|1\rangle \leftrightarrow |2\rangle$ is shown. For single particles, sub-poissonian light is emitted, which however with increasing particle number turns via coherent light emission to super-poissonian statistics. The different curves correspond to different temperatures. It can be seen that for lower temperatures, the change to super-poissonian statistics occurs at lower particle number. Non-integer particle numbers can be interpreted as mean number of particles interacting with the bath for example if a particle beam traverses a bath cavity field. In addition, in Fig. 23(a), the red triangles (blue squares) denote bunching (anti-bunching) of the emitted light. In order to determine whether the emitted light is bunched or anti-bunched, $g_{11}^{(2)}(\tau)$ needs to be calculated. Examples are shown in Fig. 23(b). Curve (i) shows bunching with super-poissonian photon statistics, (ii) anti-bunching with super-poissonian photon statistics, and (iii) is the reference result with anti-bunching for a single particle.

Interestingly, all combinations of sub-/super-poissonian statistics and bunching/anti-bunching are found in Fig. 23(a), which illustrates the fact that these two properties of the light field are independent.

Thus the given system is a versatile source of non-classical light, as required for many applications in quantum optics and information science [23]. Similar correlations can also be found between light emitted on different transitions. The cross correlations $g_{ij}^{(2)}(\tau)$ for $i \neq j$ can be shown to violate Cauchy-Schwarz inequalities for a range of bath parameters [23].

6 High-precision quantum optics in the spatial domain

In the recent past, quantum optics is advancing more and more towards a precision science. This is in particular visible in the energy-time domain, where, for example, optical clocks aim at superseding current atomic clocks [Lud08, Ros08]. Similar breakthroughs were achieved in measuring optical transition frequencies with very high precision, such as in the hydrogen 1S-2S measurement based on optical frequency combs [Han06]. These and related applications rely on quantum mechanics in order to improve performance as compared to previous, classical schemes such as the measurement of time with mechanical clocks.

The same trend also holds for the position-momentum domain. Light has been used both as a tool to measure and to manipulate with high spatial precision, for example in microscopes, telescopes, or mask-based optical lithography. The simplest techniques, however, are limited by classical constraints such as the Rayleigh criterion which states that classical uncorrelated light of wavelength λ can typically only be used to resolve or write structures of about $\lambda/2$ [Lor79]. Due to the tremendous range of applications, it is of great interest to beat such classical limits, and thus it is not surprising that in the past several decades, many methods have been developed to overcome this limit. Prominent examples for imaging techniques are near-field imaging, where the distance between object and measurement device is small enough that so-called evanescent electromagnetic waves originating from the object can be picked up by the microscope [Lew03], and various optical far field techniques [Hel07]. Mask-based optical lithography is a standard method for the production of nano- and semiconductor structures. In the following subsections, alternative methods will be presented which facilitate quantum mechanics in order to overcome classical limits both in imaging and in optical lithography.

6.1 Localization of quantum particles

6.1.1 Atom localization via multiple measurements

The question of localizing single quantum particles already started in the early days of quantum mechanics, when Heisenberg asked the question whether it would be possible to measure the position of an atom with the help of scattered light. The technological advancement since then nowadays allows to realize such thought experiments (see [Tho95] and references therein). Localization schemes under consideration here generally rely on a measurement-induced collapse of a continuous position probability distribution of the particle [Sto92]. After the measurement, the possible position reduces to a set of narrow regions with high probability. Many schemes rely on a position-dependent interaction of the quantum particle with a standing wave light field. In this case, typically several potential positions per wavelength of the driving field are obtained. These schemes that facilitate a spatially modulated light field as a reference for the position measurement, however, face a common problem. The far-field measurements typically only allow one to reconstruct the interaction strength between quantum object and field. But, due to the periodicity of the standing-wave

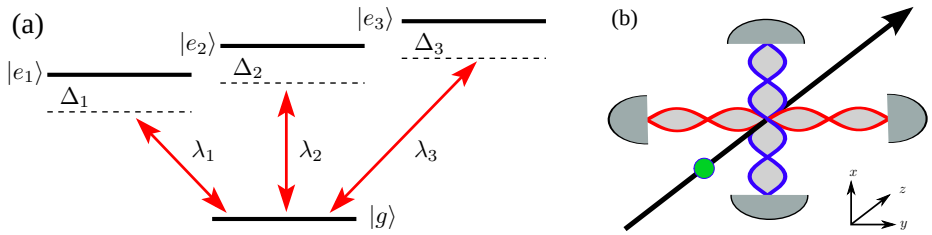

Figure 24: (a) Atomic level scheme suitable for multiple simultaneous measurements. Each light field couples to one of the transitions such that a phase shift is imprinted on the light field. (b) Possible light field setup for two-dimensional localization. The atom indicated by the green circle passes through the intersection region of two standing wave fields.

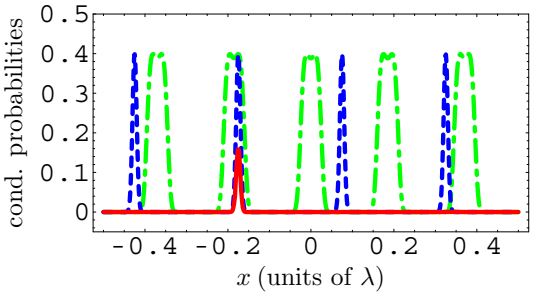

Figure 25: Conditional probabilities for the position x of a quantum particle. The dashed blue and the dash-dotted green curves show results from individual measurements. The solid red curve is the combined probability that reduces to a single position per wavelength λ.

intensity modulation, the mapping between coupling intensity and spatial position is not unique. Rather, there is a large number of potential positions within the standing-wave field that gives rise to equal coupling strength. Therefore, such measurements typically have to be accompanied by a conventional position measurement that allows one to pinpoint the position ideally to about $\lambda/2$, where λ is the wavelength of the incident light field. The quantum measurement then is used to refine this conventional position measurement to a small set of narrow potential positions within the classical range of $\lambda/2$. The goal of subsequent work was thus to reduce the number of possible positions within one wavelength in order to improve the localization (see, e.g., [Sah05]).

One way of doing so is to perform localization and center-of-mass wavefunction measurements of a single quantum particle using multiple *simultaneous* dispersive interactions of the particle with different standing wave fields [39]. The measurements turn out to be independent, if objects are considered with an internal structure consisting of a single ground state and several excited states, see Fig. 24(a). If the light fields are off-resonant with the atomic transition frequencies, then no population dynamics is induced. Rather, the atom imprints phase shifts on the light fields during the interaction, which are the observable for the position determination.

As compared to different sequential interactions, simultaneous measurements allow to reduce the required total interaction time, which is favorable because of unavoidable decoherence in the system. Also, each interaction between particle and light fields gives rise to transversal momentum changes of the particle. In multiple sequential interactions, the initial momentum becomes less and less defined. Therefore multiple simultaneous measurements allow both to increase the measurement or localization precision in a single direction and to perform multi-dimensional measurements

or localization, depending on the alignment of the different standing wave fields. The increased precision occurs because each individual measurement can be translated into a probability distribution for the particle position.

Example distributions corresponding to two different measurements are indicated as the dash-dotted green and the dashed blue curve in Fig. 25. Different probability distribution can then be combined to a total position distribution conditioned on the outcome of all measurements. Ideally, the total distribution reduces to a single peak per wavelength, as it is the case for the solid red curve in Fig. 25.

Apart from an improved localization in one spatial dimension, multi-dimensional localization is possible via simultaneous measurements with perpendicular standing wave fields as shown in Fig. 24.

6.1.2 Localization of atomic ensembles via superfluorescence

In view of the general trend in science towards more complex systems, the question arises whether current localization schemes are also applicable for larger quantum systems. It turns out that localization is possible for small ensembles of interacting quantum particles via the light scattered from a standing wave field [44]. A suitable setup is shown in Fig. 26. The linear dimension of the ensemble is assumed to be smaller than the relevant optical wavelength, such that the Dicke limit applies [Dic54]. The scattered light intensity is proportional to the number of atoms in the ensemble squared, which is a signature of superfluorescence. As in the single particle case, the fluorescence intensity is a function of the position of the ensemble in the standing wave field. For example, at the nodes, the ensemble is not driven and no light is scattered. But while in the single-particle case the fluorescence intensity slowly increases when moving the particle away from the nodes, the ensemble exhibits a very narrow dip to zero intensity at the nodes of the standing wave field. Examples for the intensity profiles found for different numbers of atoms in the ensemble are shown in Fig. 27. This narrowing arising from the collective speed-up of the system dynamics. The width of this dip depends on the particle number, and can be decreased by increasing the light intensity and a suitable choice of the standing wave frequency.

Therefore a coincidence of ensemble position and standing wave node gives precise spatial information via the absence of fluorescence light. This is in contrast to previous localization schemes, where the measurement relied on the spectrum of non-vanishing fluorescence light. By suitably tailoring the fluorescence profile via the standing wave parameters, moving the standing wave nodes via phase shifts and continuously monitoring the fluorescence intensity, the ensemble position can be identified. For example, in the upper figure of Fig. 26, the ensemble is at a random position inside the standing wave, and scatters light into the detector. Then the phase of the standing wave is shifted until the fluorescence ceases. In this case, the ensemble is known to be at a node of the standing wave, see the lower panel of Fig. 26.

Generalizations of this scheme can be used to measure the position of ensembles

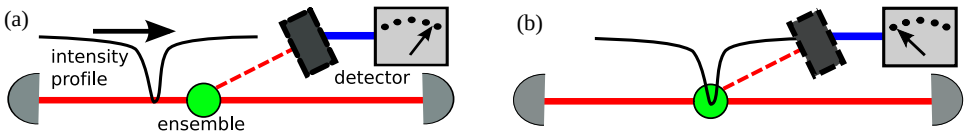

Figure 26: Localization of an ensemble via scanning-dip spectroscopy of scattered superfluorescence light. The ensemble (green circle) scatters light out of the driving cavity field, as shown in (a). The intensity of the scattered light sensitively depends on the position of the ensemble relative to the standing light field nodes. A phase shift of the standing wave allows to determine coincidences of ensemble positions and standing wave nodes with high precision by the drop in intensity as indicated in (b).

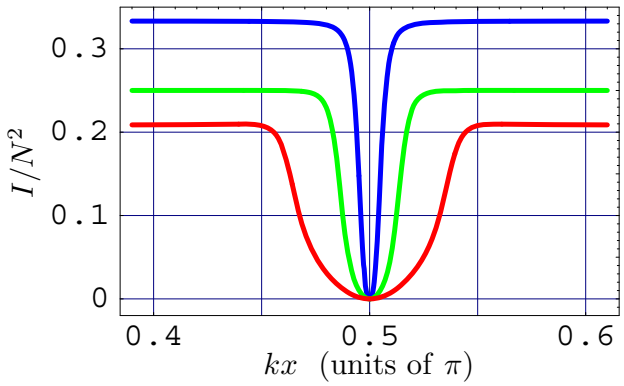

Figure 27: Position-dependent fluorescence intensity of an ensemble of atoms. k is the wavevector, x the position of the ensemble, and $k\,x = \pi/2$ corresponds to a node of the standing wave field. N is the number of atoms, which is $N = 2$ for the red curve, $N = 4$ for the green curve, and $N = 8$ for the blue curve.

passing the cavity field, the distance between two ensembles, or the diameter of an ensemble [44].

6.1.3 Interparticle distance measurements beyond classical limit

Besides the precise position measurement of quantum objects, interparticle distance measurements are a fundamental element for the spatial analysis of quantum systems. The distance measurement between two quantum objects can also be seen as an archetype system for the analysis of quantum mechanical optical resolution enhancement. A number of sophisticated schemes have been devised to subsequently improve spatial resolution from $\lambda/2$ in steps of improvement by a factor of 2 down to $\lambda/16$ (see, e.g. [Mut04] and references therein). These schemes, however, do not consider the particle interaction, and do not scale easily to higher resolution. Alternatively, a method was proposed to reach sub-wavelength resolution that is essentially based on the possibility to individually address the two nearby particles [Bet95]. This idea was subsequently realized in a landmark experiment of Hettich et al. [Het02]. They combined near-field and far-field fluorescence spectroscopy techniques, using the fluorescence spectrum to label different molecules inside an inhomogeneous external electrical field. They also noticed the existence of the dipole-dipole interaction between the adjacent objects [Fic04] and used it to correct the measurement result. These observations paved the road for nanometer distance measurements using optical illuminating far-field imaging only.

The general setup considered here is shown in Fig. 28. Two nearby quantum systems modelled by two-level atoms are driven near-resonantly by a standing wave laser field. A detector measures the far field resonance fluorescence spectrum [27]. In a standing wave field, the effective driving field strength depends on the particle positions. Each particle generates sharp sideband peaks in the spectrum, with frequencies directly related to the driving strengths and thus to the positions. For sub-wavelength distances, the two particles dipole-dipole interact and can no longer be considered independent [41]. This dipole-dipole interaction energy depends on the interparticle distance and can be extracted from the fluorescence spectrum, providing the desired distance information. Thus both position and distance can be recovered from the spectrum. Fig. 29(a) shows a typical resonance fluorescence spectrum for an intermediate distance range $\lambda/30 < r_{12} < \lambda/10$. Together with the central peak, the two sideband groups at $\pm 50\gamma$ and $\pm 130\gamma$ can be interpreted as the Mollow resonance fluorescence spectra of the two atoms driven with different coupling strengths. The splitting of

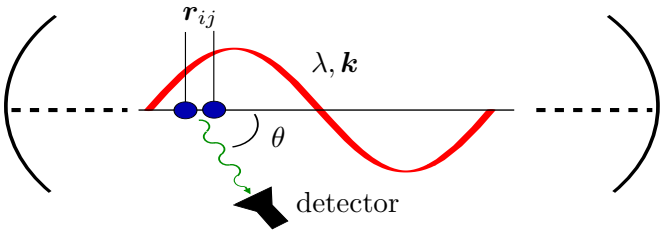

Figure 28: General setup for illuminating far-field measurements of interparticle distances. The two particles are driven by a standing wave field indicated by the red sinusoidal wave and created, e.g., inside an optical cavity. The atom pair scatters light out of the standing wave field mode that is measured by a detector.

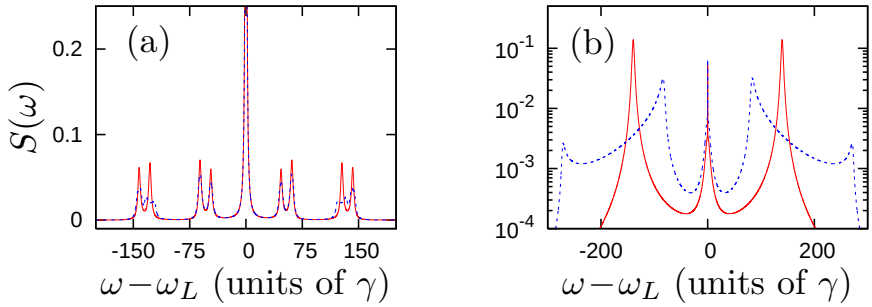

Figure 29: (a,b) Fluorescence spectrum of two nearby atoms driven by a near-resonant standing-wave laser field. The interparticle distance is (a) $r_{12} = 0.09\lambda$, (b) $r_{12} = 0.035\lambda$. Solid line: fixed distance; dashed line: average over harmonic oscillation around the equilibrium distance with an amplitude of $\pm 0.007\lambda$.

each sideband peak into two sub-peaks is due to the dipole-dipole interaction. Thus, all coupling strengths can be directly obtained from the spectrum. Fig. 29(b) show the small-distance case $r_{12} \approx \lambda/30$, where the dipole-dipole interaction dominates. In this case, the two peaks are separated by the dipole-dipole energy, and the standing wave driving leads to a barely visible splitting of both peaks. For such small distances, oscillations of the particles around their equilibrium positions become relevant, but do not spoil the measurement since spatial information can still be extracted from the spectrum. For example, in Fig. 29(b), the averaged spectrum emitted by oscillating particles contains a further splitting of the spectral peaks, with maxima corresponding to the classical turning points of the oscillation.

With the presented technique, interparticle distances can be measured down to small fractions of the involved light wavelength, and prior knowledge of the approximate distance is not required as long as it is below the wavelength scale. Using a similar setup, sub-wavelength localization is also possible via second-order correlation function measurements [25].

6.2 Resonant interferometric lithography

The miniaturization of nano- and semiconductor structures generated by optical lithography is necessary to maintain the current pace of technological innovation. Optical lithography employs a photoresist applied on top of a substrate material, that is exposed using an intensity-patterned light field. A subsequent etching process then allows to separate exposed parts of the resist from the non-exposed parts and thus to create structures reflecting the light pattern in the substrate. Classically, optical lithography is limited by diffraction just as optical imaging. Improvement is possible by increasing

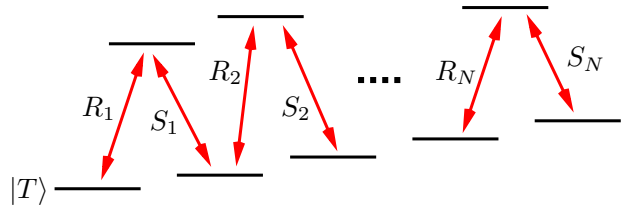

Figure 30: The internal structure that is used to model the photoresist. $|T\rangle$ is the target state that can be selectively transferred to the exposed state, e.g., via ionization. R_n and S_n ($n \in \{1, \ldots, N\}$) indicate standing wave field Rabi frequencies.

the light frequency, by making better use of the light source e.g. by immersing the target material in fluids, or by novel, alternative lithography methods.

A particular alternative method is interference lithography [Bru98]. It aims at creating sequences of closely-spaced features similar to the fringe pattern in a double-slit experiment. Patterns of different frequencies can then be combined to a desired target image using techniques based on Fourier decomposition [Sun07]. Thus, in contrast to imaging lithography, it does not work with a mask. Several schemes in the literature allow to improve the spatial resolution of interference lithography beyond classical limit [Bot00, Ben04, Pe'04, Hem06, Sun07]. The approach of quantum lithography [Bot00] is based on entangled photon-number states that are experimentally difficult to generate and sustain. In order to overcome this difficulty, other approaches achieve the desired resolution enhancement via classical coherent light pulses [Ben04, Pe'04]. These approaches suffer from a reduced visibility of the generated structures, which could be improved in [Hem06, Sun07]. In this reference, subwavelength resolution was accomplished by correlating wave vector and frequency in a narrow band multiphoton detection process. All of these methods have in common, however, that they are based on N-photon absorption, and therefore require high light field intensities which hampers an experimental realization.

To overcome this difficulty, it was shown that sub-wavelength resolution can be obtained relying entirely on resonant light-matter interactions [49]. Then, very weak driving fields can be used. The key idea of the method is to apply standing wave light fields to the target material in such a way that a position-dependent dark state in the medium is generated. For this, consider a medium as shown in Fig. 30, which can be characterized as a $N \times \Lambda$ scheme with N instances of the archetype three-level Λ setup. It is assumed that one of the states, denoted as the target state $|T\rangle$, can selectively be transfered to the exposed state, e.g., by ionization. Thus, the observable of interest is the spatial dependence of the population of $|T\rangle$. Each transition is driven resonantly by a standing wave laser field R_i or S_i. The system then evolves into a dark state $|D\rangle$ in direct generalization of the well-known dark state in a three-level system in Λ-configuration [Scu97]. For a specific light field configuration

$$\mathcal{S}_n(z) = S_n \sin[k_0 z + (n-1)\pi/N]\,, \qquad \mathcal{R}_n(z) = R_n \sin[k_0 z + (2n-1)\pi/(2N)]\,, \quad (14)$$

with Rabi frequencies $|R_1| = |S_N| = \eta\Omega_0$, and $|R_N| = |S_1| = |R_n| = |S_n| = \Omega_0$ ($1 < n < N$), where $0 < \eta \ll 1$ is a small parameter, the target state acquires a position-dependent population given by

$$|\langle T|D\rangle|^2 = \frac{1}{2}[1 - \cos(2Nk_0 z)] + \mathcal{O}(\eta^2)\,. \quad (15)$$

Thus, the population of the target state displays periodic oscillations with full visibility and with a spacing of the population maxima given by $\lambda/(2N)$. This corresponds to an improvement in spatial resolution by a factor of N as compared to the spatial modulation of the light fields and to the Rayleigh criterion. By choosing different

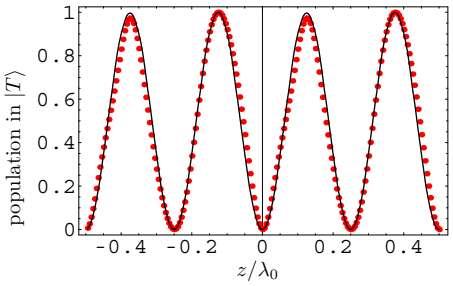

Figure 31: Medium response to the applied standing wave fields. Solid line, without ground state decoherence. Dotted line, with all ground state decoherence rates set to 5γ. Other parameters are $\eta = 1/25$, $\Omega_0 = 2.5\gamma$. γ is the natural decay rate on the transitions from the upper to the lower states.

subsets of a given extended level scheme, the various frequency components required for a Fourier composition of the desired pattern can be created. An example is shown in Fig. 31, where the solid line shows the position-dependent population pattern created in a 5-level $2 \times \Lambda$ system.

It turns out that the explanation of the subwavelength spatial population modulations entirely in terms of a dark state, which can be understood as arising from coherent population trapping (CPT) induced by the laser fields, does not provide the complete picture. CPT relies on the preservation of the ground state coherence rates, which in realistic implementations of our scheme is not guaranteed due to inevitable perturbations. Thus ground state decoherence appears to be a major limitation of the presented scheme. But it turns out that even very high ground state decoherence rates do not prohibit the scheme to work successfully. To illustrate this result, Fig. 31 also shows the corresponding result with ground state decoherence rates between any two of the ground states set to 5γ. Here, γ is the natural decay rate on the dipole-allowed transition from the excited to the ground states. It can be seen that the results with and without ground state decoherence are virtually the same. This can be understood by noting that most features in Fig. 31 can already be explained by simple optical pumping. For example, zeros in the population of the target state occur if the driving field R_1 is non-zero, while S_1 is zero. Then population is pumped out of $|T\rangle$ independent of the value of any atomic coherence. Also, the scheme is rather robust against perturbations, e.g., of the standing wave frequencies or laser field pointing errors [49]. Intensity fluctuations can be handled by deriving the various standing wave fields from the same primary laser source, as the position-dependent dark state only depends on relative Rabi frequencies.

To produce higher harmonics of the incident writing fields, an extended energy level scheme is required. This suggests two possible candidate systems. One possible realization involves the selective exposure of the target resist conditioned on the internal state of atoms that pass through the light fields before hitting the target surface and thus acquire a position-dependent population pattern as in atomic resonance lithography [Thy05]. Suitable level structures can be found, e.g. in ^{85}Rb and ^{87}Rb [Bal05]. In this method, a resolution limitation arises from the center of mass motion of atoms in the gas. A second potential realization is the direct exposure of a photoresist on a surface, such that no center of mass motion occurs. Suitable coherence times have already been demonstrated in other solid state systems, such as between spin states in doped solids [Tur01]. Also coherent population transfer has been demonstrated [Kle07]. The temperature of the target material must be chosen such that sufficient ground state coherence times are obtained [Tur02, Got06] while the resonances are broad enough for a simultaneous driving [Kol05]. Ideally, different vibrational transitions could be utilized to achieve the desired level scheme [Hem06].

7 Nuclear quantum optics

While quantum optics usually entails electronic excitations in atoms via coupling to light fields, it is important to note that the theoretical description employed are typically based on models that are valid beyond the scope of atomic quantum optics. Thus the question arises whether the abundance of successful schemes in quantum optics can be transferred to different physical systems.

One candidate field could be nuclear physics, with the aim to enhance preparation, control or detection methods. Traditionally, however, this possibility has mostly been dismissed because the direct laser-nucleus interaction strength is small. But with the advent of novel super-intense coherent light sources both in the visible and in the x-ray frequency regime [Col06], this negligence needs revision. Two cases have to be distinguished. First, the resonant interaction of coherent light with nuclear transitions, where the matching of x-ray photon and transition frequency is potentially assisted by an acceleration of the target nuclei [28]. This approach is the most promising for potential applications, but demanding in terms of the light source. In this case, also the limit coherence length typical for free electron lasers needs to be considered, in contrast to quantum optics with cw lasers in the optical range which have much longer coherence lengths. The second case involves strongly off-resonant interactions, for example, of ultra-intense optical ($\omega_L \sim$ eV) laser fields with nuclear transitions [30]. Both cases, together with isomer triggering as an application for resonant excitation of nuclei [34], will be discussed in the following.

7.1 Direct resonant laser-nucleus interactions

To a good approximation, the nuclear system can be reduced to a small set of discrete energy levels as in quantum optics, depending on the decay branching ratios of the excited states. The laser-nucleus interaction can then modeled by the famous Jaynes-Cummings Hamiltonian in a master equation for the density matrix ρ including spontaneous emission with rates γ_{SE}. Additionally, a limited coherence time γ_d^{-1} of the driving laser field has to be considered, since current and upcoming high-frequency lasing facilities typically do not offer full temporal coherence [Alt06]. The master equation then reads

$$\frac{\partial \rho}{\partial t} = \frac{i}{\hbar}[H_0, \rho] - \frac{\gamma_{SE}}{2}\left([A_{eg}, A_{ge}\rho] + \text{H.c.}\right) - \gamma_d([A_{ee}, A_{ee}\rho] + \text{H.c.}) \ , \qquad (16)$$

Here, $A_{ij} = |i\rangle\langle j|$ are population or transition operators, and i, j range over all included nuclear states. Suitable nuclear systems are those with low-lying excited states such that resonant laser-driving is possible. In contrast to atomic quantum optics, higher multipole transitions such as $M1$ or $E2$ transitions can be as efficient as electric dipole allowed $E1$ transitions [51].

In order to estimate the response of the nuclei to the incident light field, the number of scattered photons is calculated. The laser parameters are chosen as planned for the upcoming European XFEL facility currently under construction at Hamburg [Alt06, The], which will deliver pulses with a duration of 100 fs and an average brilliance of 1.6×10^{25} photons/(sec mrad^2 mm^2 0.1% bandwidth). Further, a focal diameter of the laser of 20 μm is assumed together with a repetition rate of 40 kHz. For transitions below the maximum photon energy of about 12.4 keV, a solid state target with a density of 10^{20} nuclei/cm^2 is considered, and the branching ratio between radiative deexcitation and competing electronic processes is taken into account. For transitions above 12.4 keV, an acceleration of the target nuclei is required in order to match the photon and nuclear transition energy. Thus an ion beam with 2.5×10^{10} particles with bunch length of $\tau = 50$ ns in a beam of 2 mm diameter is adopted [Tah05]. The target particle density is then 5.3×10^8 cm^{-3}. For the new Synchrotron SIS100 that will be built in the future at FAIR [Fac] the beam parameters yield a particle density of 10^{11} ions/cm^3 [Tah05]. In the calculation of the photon rate per second, the latter rate

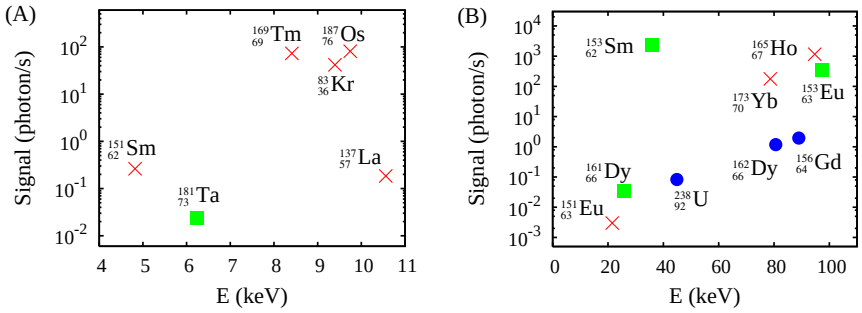

Figure 32: Signal photons per second for laser driving of nuclear transitions with energies (A) below 12.4 keV and (B) above 12.4 keV. The energy of the nuclear transition is given on the abscissa. The green squares denote $E1$ transitions, the blue circles $E2$ transitions and the red crosses $M1$ transitions. The considered experimental laser and target parameters are discussed in Sec. 7.1.

together with a matching of the ion and laser pulse repetition rates are assumed. It can be seen from Fig. 32 that between 10^{-2} and 10^{4} signal photons per second can be expected for the considered parameters, depending on the nucleus. Nevertheless it should be noted that on average the nuclei remain mostly in the ground state, because the laser parameters do not allow to exceed the low excitation regime. This is unfortunate since most coherent control schemes rely on relatively strong driving of individual transitions. A primary reason for the weak driving is the width of nuclear resonances, which is very small as compared to the spectral width of the laser pulse. Thus, most photons pass the nuclei without interacting. Still, some control schemes may succeed, for example, if the excited nuclei can selectively be addressed. Other approaches could involve the laser-driving of low-energetic transitions either in exotic nuclei or between excited states, or the artificial broadening of nuclear resonances.

The role of the limited coherence of the driving laser field generated in a free-electron laser is demonstrated in Fig. 33. In this figure, W is the population inversion, and the laser parameters are such that with full temporal coherence, the nuclei undergo few Rabi oscillations and at the end of the laser pulse remain in the excited state (black line). The other curves show identical parameters except for the limited coherence length τ_d of the light field. It can be seen that with decreasing coherence, the Rabi oscillations become less pronounced, until they finally vanish. This clearly shows that the population inversion encountered in Rabi oscillations are a direct consequence of the atomic coherence that can only be induced by coherent driving fields.

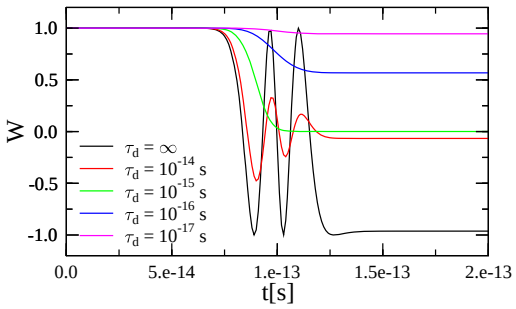

Figure 33: Influence on the limited coherence length of the light generated in a free electron laser. W is the population inversion of the nuclei, and τ_d is the coherence length of the light pulse.

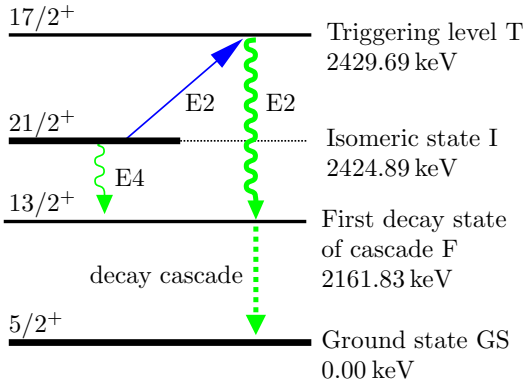

Figure 34: Partial level scheme of $^{93}_{42}$Mo. The isomeric state (I) can be excited to the triggering level (T) which subsequently decays back to I or to a level F, initiating a cascade via different intermediate states (dashed line) to the ground state (GS). The direct $I \rightarrow F$ decay is a strongly hindered $E4$ transition.

7.2 Isomer triggering via resonant excitation of the nucleus

An interesting application for the controlled transfer of nuclear population as discussed in Sec. 7.1 is given by so-called isomers. Isomers are long-lived metastable nuclear states. Triggering the decay of such isomers via an excitation to a freely radiating state releases the energy difference between the excitation energy and the transition energy to the nuclear ground state, which can be large. Thus it is not surprising that isomers have been studied in the context of so-called nuclear batteries that would allow to release nuclear energy on demand without fission or fusion. But isomers also play an important role in the formation of elements and the evolution of the universe [Wal99]. Isomer triggering is schematically presented in Fig. 34 for the case of ^{93}Mo, and can occur via a number of nuclear excitation mechanisms such as photoexcitation, Coulomb excitation or coupling to the atomic shells.

Motivated by the need to identify efficient energy release mechanisms, triggering by coupling to the atomic shell via nuclear excitation by electron capture (NEEC) and triggering via x-ray photons are compared. NEEC is a resonant process in which an electron is captured into a bound state of a highly-charged ion with the simultaneous excitation of the nucleus. In the following, energy release is studied via the nearest triggering level lying above the metastable state that has been either experimentally confirmed or for which the corresponding transition is theoretically predicted. Low-lying triggering levels are desirable for obtaining high energy gain and facilitating the excitation to the triggering level.

Results for few isomers are summarized in Table 1. The total resonance strength $S^{I\rightarrow F}_{\mathrm{NEEC}}$ is the integral of the total cross section σ for NEEC over the continuum electron energy, followed by the decay of the triggering level to the state F. The NEEC rate is calculated using a rigorous treatment of the electron-nucleus interaction following the formalism developed in [Pál06]. In comparison, x-ray excitation resonance strengths $S^{I\rightarrow F}_{\mathrm{x-ray}}$ using the same triggering levels are also presented. It can be seen that the NEEC nuclear excitation mechanism is more efficient than photo-triggering, except for $^{189}_{76}$Os. A further comparison for $^{242}_{95}$Am with other excitation mechanisms shows that NEEC is the most efficient mechanism for this isotope, in contrast to previous predictions [Zad02].

Up to now, NEEC could not be observed mostly due to the strong atomic background and the narrow nuclear state widths [Mor04]. But isomer triggering via NEEC has the advantage that the excitation and the signal photon energies can be very different, such that much of the background can be suppressed. Using realistic parameters of the future GSI facility in Darmstadt, a reaction rate of 6.5×10^{-2} s^{-1} for the NEEC

Table 1: Total resonance strengths S (in b eV) for NEEC and x-ray triggering of isomers. E_I and E_T are the isomeric state and triggering level energies, respectively.

${}^{A}_{Z}\mathrm{X}$	E_I (keV)	E_T (keV)	$S^{I\to F}_{\mathrm{NEEC}}$	$S^{I\to F}_{\mathrm{x-ray}}$
${}^{93}_{42}\mathrm{Mo}$	2424.89	2429.69	9.1×10^{-6}	1.4×10^{-8}
${}^{152}_{63}\mathrm{Eu}$	45.599	65.296	3.4×10^{-4}	6.5×10^{-5}
${}^{178}_{72}\mathrm{Hf}$	2446.05	2573.5	2.0×10^{-7}	5.4×10^{-8}
${}^{189}_{76}\mathrm{Os}$	30.812	216.661	1.2×10^{-3}	2.2×10^{-2}
${}^{204}_{82}\mathrm{Pb}$	2185.79	2264.33	4.9×10^{-5}	8.7×10^{-6}
${}^{235}_{92}\mathrm{U}$	0.076	51.709	1.3×10^{-1}	1.3×10^{-2}
${}^{242}_{95}\mathrm{Am}$	48.60	52.70	3.6×10^{-3}	2.4×10^{-8}

triggering of ${}^{235\mathrm{m}}\mathrm{U}$ and of 1.1×10^{-3} s^{-1} for the case of ${}^{189\mathrm{m}}\mathrm{Os}$ is obtained [34].

7.3 Off-resonant laser-nucleus interactions

In addition to near-resonant direct driving of nuclei discussed in Sec. 7.1, here strongly off-resonant interactions are considered, for example, of ultra-intense optical ($\omega_L \sim$ eV) laser fields with nuclear transitions [30]. The dynamical nuclear Stark shift relative to the transition frequency can be comparable to typical shifts in atomic physics already below the critical field strength $I \approx 10^{29}$ W/cm^2. Variations of standard nuclear physics parameters, such as the proton density, the shape, or the radius, can be expected at or above the critical field strength. With currently available laser intensities, a direct observation of the induced Stark shifts would be challenging. But off-resonant interactions may be of relevance in indirect laser-nucleus interactions via secondary particles, if the required field strengths are reached in the intermediate step.

A Complete list of publications

Refereed journals and conference proceedings

[1] J. Evers and C. H. Keitel, *Spontaneous emission suppression on arbitrary atomic transitions*, Phys. Rev. Lett. **89**, 163601 (2002).

[2] J. Evers, D. Bullock and C. H. Keitel, *Dark state suppression and narrow fluorescent feature in a laser-driven Lambda-atom*, Opt. Commun. **209**, 173 (2002).

[3] U. D. Jentschura, J. Evers, C. H. Keitel and K. Pachucki, *A problematic set of two-loop self-energy corrections*, New J. Phys. **4**, 49 (2002).

[4] J. Evers and C. H. Keitel, *Narrow spectral features in resonance fluorescence with a single monochromatic laser field*, Phys. Rev. A **65**, 033813 (2002).

[5] D. Bullock, J. Evers and C. H. Keitel, *Modifying spontaneous emission via interferences from incoherent pump fields*, Phys. Lett. A **307**, 8 (2003).

[6] M. Macovei, J. Evers and C. H. Keitel, *Phase-control of collective quantum dynamics*, Phys. Rev. Lett. **91**, 233601 (2003).

[7] U. D. Jentschura, J. Evers, M. Haas and C. H. Keitel, *Lamb Shift of Laser-Dressed Atomic States*, Phys. Rev. Lett. **91**, 253601 (2003).

[8] J. Evers and C. H. Keitel, *Narrow Spectral Features in Resonance Fluorescence in Laser-Driven Atomic Few-Level Systems*, in "Interactions in ultracold gases", Ed. M. Weidemüller and C. Zimmermann, Wiley-VCH, Berlin, 2003.

[9] J. Evers and C. H. Keitel, *Spontaneous-emission suppression via multiphoton quantum interference*, J. Phys. B: At. Mol. Opt. Phys. **37**, 2771 (2004).

[10] M. A. Macovei and J. Evers, *Phase dependence of collective fluorescence via interferences from incoherent pumping*, Opt. Comm. **240**, 379 (2004).

[11] J. Evers and C. H. Keitel, *Reply to Comment on J. Evers and C. H. Keitel, Phys. Rev. Lett. 89, 163601 (2002)*, Phys. Rev. Lett. **92**, 159303 (2004).

[12] J. Evers and C. H. Keitel, *Double-EIT ground-state laser cooling without blue-sideband heating*, Europhys. Lett. **68**, 370 (2004).

[13] M. Macovei, J. Evers and C. H. Keitel, *Magnetic and thermal influences on collective resonance fluorescence*, Europhys. Lett. **68**, 391 (2004).

[14] J. Evers, U. D. Jentschura and C. H. Keitel, *Relativistic and radiative corrections to the Mollow spectrum*, Phys. Rev. A **70**, 062111 (2004).

[15] U. D. Jentschura, E.-O. Le Bigot, J. Evers, P. J. Mohr and C. H. Keitel, *Relativistic and Radiative Energy Shifts for Rydberg States*, J. Phys. B: At. Mol. Opt. Phys. **38**, S97 (2005).

[16] U. D. Jentschura, J. Evers and C. H. Keitel, *Radiative corrections to multi-level Mollow-type spectra*, Laser Phys. **15**, 37 (2005).

[17] J. Evers, U. D. Jentschura, M. Macovei, and C. H. Keitel, *Vacuum-mediated incoherent processes in coherently prepared media*, in "Fluctuations and Noise in Photonics and Quantum Optics III", ed. P. R. Hemmer, J. R. Gea-Banacloche, P. Heszler, Sr., M. S. Zubairy, Proceedings of SPIE Vol. **5842** (SPIE, Bellingham, WA, 2005), p. 241-255.

[18] U. Akram, J. Evers and C. H. Keitel, *Multiphoton quantum interference on a dipole-forbidden transition*, J. Phys. B: At. Mol. Opt. Phys. **38**, L69 (2005).

[19] M. Macovei, J. Evers and C. H. Keitel, *Coherent manipulation of collective three-level systems*, Phys. Rev. A **71**, 033802 (2005).

[20] G.-X. Li, J. Evers and C. H. Keitel, *Low-frequency-field induced spontaneous-emission interference in a two-level atom placed in an anisotropic photonic crystal*, J. Phys. B: At. Mol. Opt. Phys. **38**, 1435 (2005).

[21] U. D. Jentschura and J. Evers, *Some Recent Advances in Bound-State Quantum Electrodynamics*, Can. J. Phys. **83**, 375 (2005)

[22] J. Evers, *Phase-dependent interference mechanisms in a three-level Λ system driven by a quantized laser field*, J. Mod. Opt. **52**, 2699 (2005).

[23] M. Macovei, J. Evers and C. H. Keitel, *Quantum correlations of an atomic ensemble via an incoherent bath*, Phys. Rev. A **72**, 063809 (2005).

[24] M. Mahmoudi and J. Evers, *Light propagation through closed-loop atomic media beyond the multiphoton resonancecondition*, Phys. Rev. A. **74**, 063827 (2006).

[25] J.-T. Chang, J. Evers and M. S. Zubairy, *Distilling two-atom distance information from intensity-intensity correlation function*, Phys. Rev. A **74**, 043820 (2006).

[26] M. Kiffner, J. Evers and C. H. Keitel, *Interference in the resonance fluorescence of two incoherently coupled transitions*, Phys. Rev. A **73**, 063814 (2006).

[27] J.-T. Chang, J. Evers, M. O. Scully and M. S. Zubairy, *Measurement of the separation between atoms beyond classical limit*, Phys. Rev. A **73**, 031803(R) (2006) (2006).

[28] T. J. Bürvenich, J. Evers and C. H. Keitel, *Nuclear quantum optics with x-ray laser pulses*, Phys. Rev. Lett. **96**, 142501 (2006).

[29] M. Kiffner, J. Evers and C. H. Keitel, *Quantum interference enforced by time-energy complementarity*, Phys. Rev. Lett. **96**, 100403 (2006).

[30] T. J. Bürvenich, J. Evers, and C. H. Keitel, *Dynamic nuclear Stark shift in superintense laser fields*, Phys. Rev. C **74**, 044601 (2006).

[31] J. Evers, M. Kiffner, M. Macovei and C. H. Keitel, *Geometry-dependent dynamics of two Λ-type atoms via vacuum-induced coherences*, Phys. Rev. A **73**, 023804 (2006).

[32] M. Macovei, J. Evers, G.-X. Li, and C. H. Keitel, *Strong-field spatial interference in a tailored electromagnetic bath*, Phys. Rev. Lett. **98**, 043602 (2007).

[33] A. Di Piazza, C. Müller, J. Evers, K. Z. Hatsagortsyan, and C. H. Keitel, *QED, nuclear and high-energy processes in extremely strong laser pulses*, in "ILIAS Ion and Laser beam Interaction and Application Studies", Progress Report No. 2 of the PHELIX theory group, ed. P. Mulser, T. Schlegel, GSI Report 2007-03, February 2007, 19-25 (GSI, Darmstadt, Germany, 2007) (GSI).

[34] A. Pálffy, J. Evers and C. H. Keitel, *Isomer triggering via nuclear excitation by electron capture*, Phys. Rev. Lett. **99**, 172502 (2007).

[35] M. Kiffner, J. Evers and C. H. Keitel, *Breakdown of the few-level approximation in dipole-dipole interacting systems*, in "Noise and Fluctuations in Photonics, Quantum Optics, and Communications", ed. L. Cohen, Proceedings of SPIE Vol. **6603** (SPIE, Bellingham, WA, 2007) (SPIE).

[36] M. Macovei, J. Evers, and M. S. Zubairy, *Localization of a small collection of fluorescing atoms*, in "Noise and Fluctuations in Photonics, Quantum Optics, and Communications", ed. L. Cohen, Proceedings of SPIE Vol. **6603** (SPIE, Bellingham, WA, 2007) (SPIE).

[37] J. Evers, M. Mahmoudi and M. Macovei, *Quantum interference in light scattering and propagation*, in "Noise and Fluctuations in Photonics, Quantum Optics, and Communications", ed. L. Cohen, Proceedings of SPIE Vol. **6603** (SPIE, Bellingham, WA, 2007) (SPIE).

[38] A. Di Piazza, K. Z. Hatsagortsyan, J. Evers, and C. H. Keitel, *Vacuum fluctuations and nuclear quantum optics in strong laser pulses*, in "Noise and Fluctuations in Photonics, Quantum Optics, and Communications", ed. L. Cohen, Proceedings of SPIE Vol. **6603** (SPIE, Bellingham, WA, 2007) (SPIE).

[39] J. Evers, S. Qamar, and M. S. Zubairy, *Atom localization and center-of-mass wave function determination via multiple simultaneous quadrature measurements*, Phys. Rev. A **75**, 053809 (2007).

[39] J. Evers, *Spatial Measurements Beyond Classical Limit*, in International Conference on Quantum Information Technical Digest on CD-ROM (The Optical Society of America, Washington, DC, 2007), IThC5.

[40] G.-Y. Kryuchkyan, U. D. Jentschura, J. Evers and C. H. Keitel, *Laser-Induced Dynamic Radiative Corrections in the Dressed-State and in the Floquet Picture*, J. Mod. Opt. **54**, 1481 (2007).

[41] M. Kiffner, J. Evers and C. H. Keitel, *Breakdown of the few-level approximation in collective systems*, Phys. Rev. A **76**, 013807 (2007).

[42] M. Kiffner, M. S. Zubairy, J. Evers and C. H. Keitel, *Two-mode single-atom laser as a source of entangled light*, Phys. Rev. A **75**, 033816 (2007).

[43] M. Kiffner, J. Evers and C. H. Keitel, *Coherent control in a decoherence-free subspace of a collective multi-level system*, Phys. Rev. A **75**, 032313 (2007).

[44] M. Macovei, J. Evers, C. H. Keitel, and M. S. Zubairy, *Localization of atomic ensembles via superfluorescence*, Phys. Rev. A **75**, 033801 (2007).

[45] J. Evers, M. Kiffner and C. H. Keitel, *Quantum Control of Interacting Multiatom Systems*, Proceedings of the International Conference on Computational Methods in Science and Engineering 2007 (ICCMSE 2007), AIP Conf. Proc. **963**, 756 (2007).

[46] M. Mahmoudi, R. Fleischhaker, M. Sahrai, and J. Evers, *Group velocity control in the ultraviolet domain via interacting dark-state resonances*, J. Phys. B: At. Mol. Opt. Phys. **41**, 025504 (2008).

[47] C. Müller, A. Di Piazza, A. Shahbaz, T. J. Bürvenich, J. Evers, K. Z. Hatsagortsyan, and C. H. Keitel, *High-energy, nuclear, and QED processes in strong laser fields*, Laser Phys. **18**, 175 (2008).

[48] S. I. Schmid and J. Evers, *Dipole-dipole interaction between orthogonal dipole moments in time-dependent geometries*, Phys. Rev. A **77**, 013822 (2008).

[49] M. Kiffner, J. Evers, and M. S. Zubairy, *Resonant interferometric lithography beyond the diffraction limit*, Phys. Rev. Lett. **100**, 073602 (2008).

[50] R. Fleischhaker and J. Evers, *Nonlinear effects in pulse propagation through Doppler-broadened closed-loop atomic media*, Phys. Rev. A **77**, 043805 (2008).

[51] A. Pálffy, J. Evers, and C. H. Keitel, *Electric dipole-forbidden nuclear transitions driven by super-intense laser fields*, Phys. Rev. C in print (arXiv:0711.0015).

[52] M. Macovei, J. Evers, and C. H. Keitel, *Strong-field spatial intensity-intensity correlations of light scattered from regular structures of atoms*, in "Recent Research Topics and Developments in Chemical Physics: From Quantum Scale to Macroscale", ed. A. F. Terzis and E. Paspalakis, Transworld Research Network in print (2008).

[53] P. P. Orth, J. Evers, and C. H. Keitel, *Lossless negative refraction in an active dense gas of atoms*, submitted (arXiv:0711.0303).

[54] A. Ipp, A. Di Piazza, J. Evers, and C. H. Keitel, *Photon polarization as a probe for quark-gluon plasma dynamics*, submitted (arXiv:0710.5700).

[55] B. Jungnitsch and J. Evers, in preparation (2008).

Invited talks

[T1] J. Evers and C. H. Keitel, 33rd winter colloquium on the physics of quantum electronics, Snowbird, Utah, USA, 05-09.01.2003
Spontaneous emission suppression with intense low-frequency laser fields (20 min)

[T2] J. Evers, Graduiertenkolleg "Nichtlineare Optik und Ultrakurzzeitphysik", University of Kaiserslautern, Germany, 26.01.05
Control of quantum dynamics via coherences and interferences (60 min)

[T3] J. Evers, Saturday morning physics, MPI für Kernphysik, Heidelberg, Germany, 23.04.2005
Introduction to the quantum theory of atoms and photons (30 min)

[T4] J. Evers, Texas A&M University, Quantum Optics Group, Texas, USA, 17.05.2005
Quantum Interference in Laser Cooling and Collective Quantum Systems (60 min)

[T5] J. Evers and C. H. Keitel, SPIE conference on "Fluctuations and Noise in Photonics and Quantum Optics III", Austin, Texas, USA, 24-26.05.2005
Vacuum-mediated incoherent processes in coherently prepared media (30 min)

[T6] J. Evers, Käthe-Kollwitz-Gymnasium, Rostock, 22.06.2005 (MPG meeting)
Zu viele Köche verderben den Brei - warum in der Quantenwelt mehrere Wege nicht immer zum Ziel führen (90 min)

[T7] J. Evers, Gymnasium Rostocker Heide, Rövershagen, 23.06.2005 (MPG meeting)
Zu viele Köche verderben den Brei - warum in der Quantenwelt mehrere Wege nicht immer zum Ziel führen (90 min)

[T8] J. Evers, Huazhong Normal University, Wuhan, China, 07.12.2005
Vacuum-mediated processes from single-atom to many-atom systems (60 min)

[T9] J. Evers, International conference on quantum optics, Chinese University of Hong Kong, Hong Kong, 18.12.2005
Collective quantum dynamics in multi-atom systems (30 min)

[T10] J. Evers, Int. Nathiagali Summer College on Physics and Contemporary Needs/Int. Workshop on Quantum Informatics and Quantum Devices, Nathiagali, Pakistan, 01.07.2006
Precision spectroscopy and control of quantum dynamics (50 min)

[T11] J. Evers, Int. Nathiagali Summer College on Physics and Contemporary Needs/Int. Workshop on Quantum Informatics and Quantum Devices, Nathiagali, Pakistan, 30.06.2006
Quantum informatics in collective quantum systems (50 min)

[T12] J. Evers, Int. Symposium on Quantum Optics, Islamabad, Pakistan, 09-11.01.2007
One, two, many: Group dynamics in quantum optics (3 x 60 min)

[T13] J. Evers, Physics Colloquium, University of Queensland, Brisbane, Australia, 02.03.2007
Coherence and Interference in Quantum Optics (60 min)

[T14] J. Evers, Colloquium of the Graduate School of Fundamental Physics, University of Heidelberg, Heidelberg, 25.04.2007
Quantum interference from single- to many-particle quantum systems (60 min)

[T15] J. Evers, M. Macovei, M. Mahmoudi and C. H. Keitel, SPIE conference on "Noise and Fluctuations in Photonics, Quantum Optics, and Communications", Florence, Italy, 23.05.2007
Quantum interference in light scattering and propagation (30 min)

[T16] J. Evers, M. Kiffner and C. H. Keitel, Symposium on Quantum Control and Light-Matter Interactions, Corfu, Greece, 25-30.09.2007
Quantum control of interacting multiatom systems (30 min)

[T17] J. Evers, KACST Symposium on Quantum Optics and Laser Physics, King Abdul-Aziz City of Science and Technology, Riyadh, Saudi-Arabia, 16-20.02.2008
Negative refraction in active dense atomic gases (60min)

[T18] J. Evers, Institut für Laserphysik, University of Hamburg, Hamburg, 20.02.2008
Coherence and interference from single to many-particle quantum systems (45 min)

B References

[Aga74] G. S. Agarwal, in G. Hohler (Editor), *Quantum Statistical Theories of Spontaneous Emission and Their Relation to Other Approaches* (Springer, Berlin, 1974).

[Aga01] G. S. Agarwal and A. K. Patnaik, *Vacuum-induced coherences in radiatively coupled multilevel systems*, Phys. Rev. A **63**, 043805 (2001).

[Alt06] M. Altarelli *et al.*, *XFEL: The European X-Ray Free-Electron Laser. Technical Design Report* (DESY, Hamburg, 2006).

[And93] A. V. Andreev, V. I. Emel'yanov, and Y. A. Il'inskii, *Cooperative Effects in Optics. Superfluorescence and Phase Transitions* (IoP, London, 1993).

[Arn01] M. C. Arnesen, S. Bose, and V. Vedral, *Natural Thermal and Magnetic Entanglement in the 1D Heisenberg Model*, Phys. Rev. Lett. **87**, 017901 (2001).

[Bal05] V. Balić, D. A. Braje, P. Kolchin, G. Y. Yin, and S. E. harris, *Generation of Paired Photons with Controllable Waveforms*, Phys. Rev. Lett. **94**, 183601 (2005).

[Ben04] S. J. Bentley and R. W. Boyd, *Nonlinear optical lithography with ultra-high sub-Rayleigh resolution*, Optics Express **12**(23), 5735 (2004).

[Bet95] E. Betzig, *Proposed method for molecular imaging*, Opt. Lett. **20**, 237 (1995).

[Bot00] A. N. Boto, P. Kok, D. S. Abrams, S. L. Braunstein, C. P. Williams, and J. P. Dowling, *Quantum Interferometric Optical Lithography: Exploiting Entanglement to Beat the Diffraction Limit*, Phys. Rev. Lett. **85**(13), 2733 (2000).

[Bow93] C. M. Bowden and J. P. Dowling, *Near-dipole-dipole effects in dense media: Generalized Maxwell-Bloch equations*, Phys. Rev. A **47**, 1247 (1993).

[Boy92] R. W. Boyd, *Nonlinear Optics* (Academic Press, London, 1992).

[Bru98] S. R. J. Brueck, S. H. Zaidi, X. Chen, and Z. Zhang, *Interferometric lithography - from periodic arrays to arbitrary patterns*, Microelectron. Eng. **42**, 145 (1998).

[Car04] T. J. Carroll, K. Claringbould, A. Goodsell, M. J. Lim, and M. W. Noel, *Angular Dependence of the Dipole-Dipole Interaction in a Nearly One-Dimensional Sample of Rydberg Atoms*, Phys. Rev. Lett. **93**, 153001 (2004).

[Col06] W. B. Colson, J. Blau, and A. Kampouridis, Proceedings of FEL 2006, BESSY, Berlin, Germany 756 (2006).

[Cra84] D. P. Craig and T. Thirunamachandran, *Molecular Quantum Electrodynamics* (Dover Publications, Mineola, NY, 1984).

[D'A01] M. D'Angelo, M. V. Chekhova, and Y. Shih, *Two-Photon Diffraction and Quantum Lithography*, Phys. Rev. Lett. **87**, 013602 (2001).

[Dic54] R. H. Dicke, *Coherence in Spontaneous Radiation Processes*, Phys. Rev. **93**, 99 (1954).

[Dut05] M. V. G. Dutt, J. Cheng, B. Li, X. Xu, X. Li, P. R. Berman, D. G. Steel, A. S. Bracker, D. Gammon, S. E. Economou, R.-B. Liu, and L. J. Sham, *Stimulated and Spontaneous Optical Generation of Electron Spin Coherence in Charged GaAs Quantum Dots*, Physical Review Letters **94**, 227403 (2005).

[Eic93a] U. Eichmann, J. C. Bergquist, J. J. Bollinger, J. M. Gilligan, W. M. Itano, D. J. Wineland, and M. G. Raizen, *Young's Interference Experiment with Light Scattered from Two Atoms*, Phys. Rev. Lett. **70**(16), 2359 (1993).

[Eic93b] U. Eichmann, J. C. Bergquist, J. J. Bollinger, J. M. Gilligan, W. M. Itano, D. J. Wineland, and M. G. Raizen, *Young's interference experiment with light scattered from two atoms*, Phys. Rev. Lett. **70**, 2359 (1993).

[Esc01] J. Eschner, C. Raab, F. Schmidt-Kaler, and R. Blatt, *Light interference from single atoms and their mirror images*, Nature **413**, 495 (2001).

[Fac] Facility for Antiproton and Ion Research Homepage, http://www.gsi.de/fair.

[Fic02] Z. Ficek and R. Tanas, *Entangled states and collective nonclassical effects in two-atom systems*, Phys. Rep. **372**, 369 (2002).

[Fic04] Z. Ficek and S. Swain, *Simulating quantum interference in a three-level system with perpendicular transition dipole moments*, Phys. Rev. A **69**(2), 023401 (2004).

[Fic05] Z. Ficek and S. Swain, *Quantum Interference and Coherence* (Springer, New York, 2005).

[Fle05] M. Fleischhauer, A. Imamoglu, and J. P. Marangos, *Electromagnetically induced transparency: Optics in coherent media*, Rev. Mod. Phys. **77**, 633 (2005).

[Flo83] G. Floquet, *Sur les equations differentielles lineaires a coefficients periodique*, Ann. École Norm. Sup. **12**, 47 (1883).

[Flo04] M. Florescu and S. John, *Resonance fluorescence in photonic band gap waveguide architectures: Engineering the vacuum for all-optical switching*, Phys. Rev. A **69**, 053810 (2004).

[Fry00] E. S. Fry, M. D. Lukin, T. Walther, and G. R. Welch, *Four-level atomic coherence and cw VUV lasers*, Opt. Comm. **179**, 499 (2000).

[Gla07] R. J. Glauber, *Quantum Theory of Optical Coherence: selected papers and lectures* (WILEY–VCH, Weinheim, 2007).

[Got06] H. Goto and K. Ichimura, *Population transfer via stimulated Raman adiabatic passage in a solid*, Phys. Rev. A **74**, 053410 (2006).

[Gre00] C. Greiner, B. Boggs, and T. W. Mossberg, *Superradiant Emission Dynamics of an Optically Thin Material Sample in a Short-Decay-Time Optical Cavity*, Phys. Rev. Lett. **85**, 3793 (2000).

[Han06] T. W. Hansch, *Nobel Lecture: Passion for precision*, Reviews of Modern Physics **78**(4), 1297 (2006).

[Har97] S. E. Harris, *Electromagnetically Induced Transparency*, Phys. Tod. **50**, 36 (1997).

[Hel07] S. W. Hell, *Far-Field Optical Nanoscopy*, Science **316**, 1153 (2007).

[Hem06] P. R. Hemmer, A. Muthukrishnan, M. O. Scully, and M. S. Zubairy, *Quantum Lithography with Classical Light*, Phys. Rev. Lett. **96**(16), 163603 (2006).

[Het02] C. Hettich, C. Schmitt, J. Zitzmann, S. Kühn, I. Gerhardt, and V. Sandoghdar, *Nanometer Resolution and Coherent Optical Dipole Coupling of Two Individual Molecules*, Science **298**, 385 (2002).

[Ita98] W. M. Itano, J. C. Bergquist, J. J. Bollinger, D. J. Wineland, U. Eichmann, and M. G. Raizen, *Complementarity and Young's interference fringes from two atoms*, Phys. Rev. A **57**(6), 4176 (1998).

[KÖ7] J. Kästel, M. Fleischhauer, S. F. Yelin, and R. L. Walsworth, *Tunable Negative Refraction without Absorption via Electromagnetically Induced Chirality*, Phys. Rev. Lett. **99**, 073602 (2007).

[Kei93] C. H. Keitel, O. A. Kocharovskaya, L. M. Narducci, M. O. Scully, S.-Y. Zhu, and H. M. Doss, *Two mechanisms for inversionless amplification in four-level atoms with Raman pumping*, Phys. Rev. A **48**, 3196 (1993).

[Kle07] J. Klein, F. Beil, and T. Halfmann, *Robust Population Transfer by Stimulated Raman Adiabatic Passage in a Pr^{3+}:Y_2SiO_5 Crystal*, Phys. Rev. Lett. **99**, 113003 (2007).

[Koc90] O. Kocharovskaya and P. Mandel, *Amplification without inversion: The double-Λ scheme*, Phys. Rev. A **42**, 523 (1990).

[Kol05] R. Kolesov, *Coherent population trapping in a crystalline solid at room temperature*, Phys. Rev. A **72**, 051801(R) (2005).

[Kor99a] E. A. Korsunsky and D. V. Kosachiov, *Phase-dependent nonlinear optics with double-Λ atoms*, Phys. Rev. A **60**, 4996 (1999).

[Kor99b] E. A. Korsunsky, N. Leinfellner, A. Huss, S. Baluschev, and L. Windholz, *Phase-dependent electromagnetically induced transparency*, Phys. Rev. A **59**, 2302 (1999).

[Lew03] A. Lewis, H. Taha, A. Strinkovski, A. Manevitch, A. Khatchatouriants, R. Dekhter, and E. Ammann, *Near-field optics: from subwavelength illumination to nanometric shadowing*, Nat. Biotechnol. **21**, 1378 (2003).

[Li00] L. Li, X. Wang, J. Yang, G. Lazarow, J. Qi, and A. M. Lyyra, *Comment on Phys. Rev. Lett. 77, p. 1032, 1996*, Phys. Rev. Lett. **84**, 4016 (2000).

[Lid98] D. A. Lidar, I. L. Chuang, and K. B. Whaley, *Decoherence-free subspaces for quantum computation*, Phys. Rev. Lett. **81**, 2594 (1998).

[Lin05a] F. Lindner, M. G. Schatzel, H. Walther, A. Baltuska, E. Goulielmakis, F. Krausz, D. B. Milosevic, D. Bauer, W. Becker, and G. G. Paulus, *Attosecond Double-Slit Experiment*, Phys. Rev. Lett. **95**(4), 040401 (2005).

[Lin05b] F. Lindner, M. G. Schätzel, H. Walther, A. Baltuska, E. Goulielmakis, F. Krausz, D. B. Milosevic, D. Bauer, W. Becker, and G. G. Paulus, *Attosecond Double-Slit Experiment*, Phys. Rev. Lett. **95**, 040401 (2005).

[Lor79] Lord Rayleigh, *Investigations in optics with special reference to the spectroscope*, Phil. Mag. **8**, 261 (1879).

[Lou80] R. Loudon, *Non-classical effects in the statistical properties of light*, Rep. Prog. Phys. **43**, 913 (1980).

[Lud08] A. D. Ludlow, T. Zelevinsky, G. K. Campbell, S. Blatt, M. M. Boyd, M. H. G. de Miranda, M. J. Martin, J. W. Thomsen, S. M. Foreman, J. Ye, T. M. Fortier, J. E. Stalnaker, S. A. Diddams, Y. Le Coq, Z. W. Barber, N. Poli, N. D. Lemke, K. M. Beck, and C. W. Oates, *Sr Lattice Clock at 1 x 10-16 Fractional Uncertainty by Remote Optical Evaluation with a Ca Clock*, Science **319**(5871), 1805 (2008).

[Luk99] M. D. Lukin, S. F. Yelin, M. Fleischhauer, and M. O. Scully, *Quantum interference effects induced by interacting dark resonances*, Phys. Rev. A **60**, 3225 (1999).

[Mar97] M. A. G. Martinez, P. R. Herczfeld, C. Samuels, L. M. Narducci, and C. H. Keitel, *Quantum interference effects in spontaneous atomic emission: Dependence of the resonance fluorescence spectrum on the phase of the driving field*, Phys. Rev. A **55**, 4483 (1997).

[Mor02] G. Morigi, S. Franke-Arnold, and G.-L. Oppo, *Phase-dependent interaction in a four-level atomic configuration*, Phys. Rev. A **66**, 053409 (2002).

[Mor04] P. Morel, J. M. Daugas, G. Gosselin, V. Méot, and D. Gogny, *Nuclear excitation by electronic processes: NEEC and NEET effects*, Nucl. Phys. A **746**, 608c (2004).

[Mut04] A. Muthukrishnan, M. O. Scully, and M. S. Zubairy, *Quantum microscopy using photon correlations*, J. Opt. B: Quantum Semiclass. Opt. **6**, S575 (2004).

[PÓ6] A. Pálffy, W. Scheid, and Z. Harman, *Theory of nuclear excitation by electron capture for heavy ions*, Phys. Rev. A **73**, 012715 (2006).

[Pat99] A. K. Patnaik and G. S. Agarwal, *Cavity-induced coherence effects in spontaneous emissions from preselection of polarization*, Phys. Rev. A **59**, 3015 (1999).

[Pe'04] A. Pe'er, B. Dayan, M. Vucelja, Y. Silberberg, and A. A. Friesem, *Quantum lithography by coherent control of classical light pulses*, Optics Express **12**, 6600 (2004).

[Ple02] M. B. Plenio and S. F. Huelga, *Entangled Light from White Noise*, Phys. Rev. Lett. **88**, 197901 (2002).

[Ros08] T. Rosenband, D. B. Hume, P. O. Schmidt, C. W. Chou, A. Brusch, L. Lorini, W. H. Oskay, R. E. Drullinger, T. M. Fortier, J. E. Stalnaker, S. A. Diddams, W. C. Swann, N. R. Newbury, W. M. Itano, D. J. Wineland, and J. C. Bergquist, *Frequency Ratio of Al+ and Hg+ Single-Ion Optical Clocks; Metrology at the 17th Decimal Place*, Science **319**(5871), 1808 (2008).

[Sah05] M. Sahrai, H. Tajalli, K. T. Kapale, and M. S. Zubairy, *Subwavelength atom localization via amplitude and phase control of the absorption spectrum*, Phys. Rev. A **72**, 013820 (2005).

[Scu97] M. O. Scully and M. S. Zubairy, *Quantum Optics* (Cambridge University Press, Cambridge, 1997).

[Sha07] V. M. Shalaev, *Optical negative-index metamaterials*, Nature Photonics **1**, 41 (2007).

[Ska06] J. Skaag, *Fresnel Equations and the Refractive Index of Active Media*, Phys. Rev. E **73**, 026605 (2006).

[Sko01] C. Skornia, J. von Zanthier, G. S. Agarwal, E. Werner, and H. Walther, *Nonclassical interference effects in the radiation from coherently driven uncorrelated atoms*, Phys. Rev. A **64**, 063801 (2001).

[Sto92] P. Storey, M. Collett, and D. Walls, *Measurement-induced diffraction and interference of atoms*, Phys. Rev. Lett. **68**, 472 (1992).

[Sun07] Q. Sun, P. R. Hemmer, and M. S. Zubairy, *Quantum lithography with classical light: Generation of arbitrary patterns*, Phys. Rev. A **75**, 065803 (2007).

[Tah05] N. A. Tahir, C. Deutsch, V. E. Fortov, V. Gryaznov, D. H. H. Hoffmann, M. Kulish, I. V. Lomonosov, V. Mintsev, P. Ni, D. Nikolaev, A. R. Piriz, N. Shilkin, P. Spiller, A. Shutov, M. Temporal, V. Ternovoi, S. Udrea, and D. Varentsov, *Proposal for the Study of Thermophysical Properties of High-Energy-Density Matter Using Current and Future Heavy-Ion Accelerator Facilities at GSI Darmstadt*, Phys. Rev. Lett. **95**, 035001 (2005).

[The] The European X-Ray Laser project homepage, http://www.xfel.net.

[Tho95] J. E. Thomas and L. J. Wang, *Precision position measurement of moving atoms*, Phys. Rep. **262**, 311 (1995).

[Thy05] J. H. Thywissen and M. Prentiss, *Demonstration of frequency encoding in neutral atom lithography*, New J. Phys. **7**, 47 (2005).

[Tur01] A. Turukhin, V. S. Sudarshanam, M. S. Shahriar, J. A. Musser, B. S. Ham, and P. R. Hemmer, *Observation of Ultraslow and Stored Light Pulses in a Solid*, Phys. Rev. Lett. **88**, 023602 (2001).

[Tur02] A. V. Turukhin, V. S. Sudarshanam, M. S. Shahriar, J. A. Musser, B. S. Ham, and P. R. Hemmer, *Observation of Ultraslow and Stored Light Pulses in a Solid*, Phys. Rev. Lett. **70**, 023602 (2002).

[Wal99] P. M. Walker and G. D. Dracoulis, *Energy traps in atomic nuclei*, Numer. Algor. **399**, 35 (1999).

[Weg] M. Wegener, *http://www.aph.uni-karlsruhe.de/wegener* (Universität Karlsruhe).

[Xia96] H. R. Xia, C. Y. Ye, and S. Y. Zhu, *Experimental Observation of Spontaneous Emission Cancellation*, Phys. Rev. Lett. **77**, 1032 (1996).

[Xio05] J. Xiong, D.-Z. Cao, F. Huang, H.-G. Li, X.-J. Sun, and K. Wang, *Experimental Observation of Classical Subwavelength Interference with a Pseudothermal Light Source*, Phys. Rev. Lett. **94**, 173601 (2005).

[Zad02] A. A. Zadernovsky and J. J. Carroll, *Non-radiative triggering of long-lived nuclear isomers*, Hyperfine Int. **143**, 153 (2002).

[Zan97] P. Zanardi and M. Rasetti, *Noiseless Quantum Codes*, Phys. Rev. Lett. **79**, 3306 (1997).

[Zho00] P. Zhou and S. Swain, *Cavity engineering of quantum interference*, Opt. Comm. **179**, 267 (2000).

[Zhu88] Y. Zhu, A. Lezama, T. W. Mossberg, and M. Lewenstein, *Vacuum-Field Dressed-State Pumping*, Phys. Rev. Lett. **61**, 1946 (1988).

C Selected publications

(reprints removed from the online version)

M. Kiffner, J. Evers, and M. S. Zubairy,
Phys. Rev. Lett. **100**, 073602 (2008) (Link to published version)
Resonant interferometric lithography beyond the diffraction limit
(and Nature **451**, 1032 (28 February 2008), Research Highlights)
(and Physical Review Focus, 13 Feb. 2008)

S. I. Schmid and J. Evers,
Phys. Rev. A **77**, 013822 (2008) (Link to published version)
Dipole-dipole interaction between orthogonal dipole moments in time-dependent geometries

A. Pálffy, J. Evers and C. H. Keitel,
Phys. Rev. Lett. **99**, 172502 (2007) (Link to published version)
Isomer triggering via nuclear excitation by electron capture
(selected as a Phys. Rev. Lett. Editors' suggestion)

J. Evers, S. Qamar, and M. S. Zubairy,
Phys. Rev. A **75**, 053809 (2007) (Link to published version)
Atom localization and center-of-mass wave function determination via multiple simultaneous quadrature measurements

M. Macovei, J. Evers, G.-X. Li, and C. H. Keitel,
Phys. Rev. Lett. **98**, 043602 (2007) (Link to published version)
Strong-field spatial interference in a tailored electromagnetic bath

M. Mahmoudi and J. Evers,
Phys. Rev. A. **74**, 063827 (2006) (Link to published version)
Light propagation through closed-loop atomic media beyond the multiphoton resonance condition

J.-T. Chang, J. Evers, M. O. Scully and M. S. Zubairy,
Phys. Rev. A **73**, 031803(R) (2006) (Link to published version)
Measurement of the separation between atoms beyond classical limit

T. J. Bürvenich, J. Evers and C. H. Keitel,
Phys. Rev. Lett. **96**, 142501 (2006) (Link to published version)
Nuclear quantum optics with x-ray laser pulses
(and May 2006 issue of Virtual Journal of Ultrafast Science)
(and Physics News Update Number 774 # 2, April 19, 2006)
(and Science Vol. **312**, p. 661 (5 May 2006), Editors' Choice)

M. Kiffner, J. Evers and C. H. Keitel,
Phys. Rev. Lett. **96**, 100403 (2006) (Link to published version)
Quantum interference enforced by time-energy complementarity

J. Evers, M. Kiffner, M. Macovei and C. H. Keitel,
Phys. Rev. A **73**, 023804 (2006) (Link to published version)
Geometry-dependent dynamics of two Λ-type atoms via vacuum-induced coherences

M. Macovei, J. Evers and C. H. Keitel,
Phys. Rev. Lett. **91**, 233601 (2003) (Link to published version)
Phase-control of collective quantum dynamics

J. Evers and C. H. Keitel,
Phys. Rev. Lett. **89**, 163601 (2002) (Link to published version)
Spontaneous emission suppression on arbitrary atomic transitions